

Early nucleocapsid-specific T cell responses associate with control of SARS-CoV-2 in the upper airways and reduced systemic inflammation before seroconversion

Tabea M. Eser

Division of Infectious Diseases and Tropical Medicine, University Hospital; German Center for Infection Research (DZIF), Partner Site Munich

Olga Baranov

Division of Infectious Diseases and Tropical Medicine, University Hospital; German Center for Infection Research (DZIF), Partner Site Munich

Manuel Huth

Institute of Computational Biology, Helmholtz Zentrum München; Center for Mathematics, Technische Universität München

Mohamed I. M. Ahmed

Division of Infectious Diseases and Tropical Medicine, University Hospital; German Center for Infection Research (DZIF), Partner Site Munich

Flora Deák

Division of Infectious Diseases and Tropical Medicine, University Hospital; German Center for Infection Research (DZIF), Partner Site Munich

Kathrin Held

Division of Infectious Diseases and Tropical Medicine, University Hospital; German Center for Infection Research (DZIF), Partner Site Munich

Luming Lin

Division of Infectious Diseases and Tropical Medicine, University Hospital; German Center for Infection Research (DZIF), Partner Site Munich

Kami Perkayvaz

Department of Medicine I, University Hospital; German Centre for Cardiovascular Research (DZHK), Partner Site Munich Heart Alliance

Alexander Leuning

Department of Medicine I, University Hospital; German Centre for Cardiovascular Research (DZHK), Partner Site Munich Heart Alliance

Leo Nicolai

Department of Medicine I, University Hospital; German Centre for Cardiovascular Research (DZHK), Partner Site Munich Heart Alliance

Georgios Pollakis

Institute of Infection and Global Health, University of Liverpool

Marcus Buggert

Center for Infectious Medicine, Department of Medicine Huddinge, Karolinska Institutet

David A. Price

Division of Infection and Immunity, Cardiff University School of Medicine, University Hospital

Raquel Rubio-Acero

Division of Infectious Diseases and Tropical Medicine, University Hospital

Jakob Reich

Division of Infectious Diseases and Tropical Medicine, University Hospital

Philine Falk

Division of Infectious Diseases and Tropical Medicine, University Hospital

Alisa Markgraf

Division of Infectious Diseases and Tropical Medicine, University Hospital

Kerstin Puchinger

Division of Infectious Diseases and Tropical Medicine, University Hospital

Noemi Castellitti

Division of Infectious Diseases and Tropical Medicine, University Hospital; German Center for Infection Research (DZIF), Partner Site Munich

Laura Olbrich

Division of Infectious Diseases and Tropical Medicine, University Hospital; German Center for Infection Research (DZIF), Partner Site Munich

Kanika Vanshylla

Laboratory of Experimental Immunology, Institute of Virology, Faculty of Medicine and University Hospital Cologne

Florian Klein

Laboratory of Experimental Immunology, Institute of Virology, Faculty of Medicine and University Hospital Cologne

Andreas Wieser

Division of Infectious Diseases and Tropical Medicine, University Hospital; German Center for Infection Research (DZIF), Partner Site Munich; Max von Pettenkofer Institute for Hygiene and Medical Microbiology

Jan Hasenauer

Institute of Computational Biology, Helmholtz Zentrum München; Center for Mathematics, Technische Universität München; Faculty of Mathematics and Natural Sciences

Inge Kroidl**Michael Hölscher****Christof Geldmacher** (✉ geldmacher@lrz.uni-muenchen.de)

Division of Infectious Diseases and Tropical Medicine, University Hospital; German Center for Infection Research (DZIF), Partner Site Munich

Research Article

Keywords:

Posted Date: November 1st, 2022

DOI: <https://doi.org/10.21203/rs.3.rs-2222184/v1>

License:   This work is licensed under a Creative Commons Attribution 4.0 International License.

[Read Full License](#)

1 **RESEARCH REPORT**

2
3 **Early nucleocapsid-specific T cell responses associate with control of**
4 **SARS-CoV-2 in the upper airways and reduced systemic inflammation**
5 **before seroconversion**

6
7 **Tabea M. Eser^{1,2}, Olga Baranov^{1,2}, Manuel Huth^{3,4}, Mohammed I. M. Ahmed^{1,2},**
8 **Flora Deák^{1,2}, Kathrin Held^{1,2}, Luming Lin^{1,2}, Kami Pekayvez^{5,6}, Alexander**
9 **Leunig^{5,6}, Leo Nicolai^{5,6}, Georgios Pollakis⁷, Marcus Buggert⁸, David A. Price^{9,10},**
10 **Raquel Rubio-Acero¹, Jakob Reich¹, Philine Falk¹, Alissa Markgraf¹, Kerstin**
11 **Puchinger¹, Noemi Castelletti^{1,2}, Laura Olbrich^{1,2}, Kanika Vanshylla¹¹, Florian**
12 **Klein^{11,12,13}, Andreas Wieser^{1,2,14}, Jan Hasenauer^{3,4,15}, Inge Kroidl^{1,2}, Michael**
13 **Hoelscher^{1,2} and Christof Geldmacher^{1,2,*}**

14
15 ¹Division of Infectious Diseases and Tropical Medicine, University Hospital, LMU
16 Munich, 81377 Munich, Germany

17 ²German Center for Infection Research (DZIF), Partner Site Munich, 81377 Munich,
18 Germany

19 ³Institute of Computational Biology, Helmholtz Zentrum München, 85764
20 Neuherberg, Germany

21 ⁴Center for Mathematics, Technische Universität München, 85748 Garching,
22 Germany

23 ⁵Department of Medicine I, University Hospital, LMU Munich, 81377 Munich,
24 Germany

25 ⁶German Centre for Cardiovascular Research (DZHK), Partner Site Munich Heart
26 Alliance, 81377 Munich, Germany

27 ⁷Institute of Infection and Global Health, University of Liverpool, Liverpool L69 2BE,
28 UK

29 ⁸Center for Infectious Medicine, Department of Medicine Huddinge, Karolinska
30 Institutet, Karolinska University Hospital Huddinge, 141 86 Stockholm, Sweden

31 ⁹Division of Infection and Immunity, Cardiff University School of Medicine, University
32 Hospital, Heath Park, Cardiff CF14 4XN, UK

33 ¹⁰Systems Immunity Research Institute, Cardiff University School of Medicine,
34 University Hospital, Heath Park, Cardiff CF14 4XN, UK

35 ¹¹Laboratory of Experimental Immunology, Institute of Virology, Faculty of Medicine
36 and University Hospital Cologne, University of Cologne, 50931 Cologne, Germany

37 ¹²German Center for Infection Research (DZIF), Partner Site Bonn-Cologne, 50937
38 Cologne, Germany

39 ¹³Center for Molecular Medicine Cologne (CMMC), University of Cologne, 50931
40 Cologne, Germany

41 ¹⁴Max von Pettenkofer Institute for Hygiene and Medical Microbiology, LMU Munich,
42 81377 Munich, Germany

43 ¹⁵Faculty of Mathematics and Natural Sciences, University of Bonn, 53113 Bonn,
44 Germany

45

46 *Correspondence should be addressed to Christof Geldmacher (geldmacher@lrz.uni-
47 muenchen.de).

48

49

50

51

52

53

54

55

56

57

58

59

60

61

62

63

64

65

66

67

68

69 **SUMMARY**

70 Despite intensive research since the emergence of SARS-CoV-2, it has remained
71 unclear precisely which components of the early immune response protect against the
72 development of severe COVID-19. To address this issue, we performed a
73 comprehensive immunogenetic and virologic analysis of nasopharyngeal and
74 peripheral blood samples obtained during the acute phase of infection with SARS-CoV-
75 2. We found that soluble and transcriptional markers of systemic inflammation peaked
76 during the first week after symptom onset and correlated directly with the upper airways
77 viral loads (UA-VLs), whereas the contemporaneous frequencies of circulating viral
78 nucleocapsid (NC)-specific CD4⁺ and CD8⁺ T cells correlated inversely with various
79 inflammatory markers and UA-VLs. In addition, we observed high frequencies of
80 activated CD4⁺ and CD8⁺ T cells in acutely infected nasopharyngeal tissue, many of
81 which expressed genes encoding various effector molecules, such as cytotoxic
82 proteins and IFN- γ . The presence of functionally active T cells in the infected epithelium
83 was further linked with common patterns of gene expression among virus-susceptible
84 target cells and better local control of SARS-CoV-2. Collectively, these results
85 identified an immune correlate of protection against SARS-CoV-2, which could inform
86 the development of more effective vaccines to combat the acute and chronic illnesses
87 attributable to COVID-19.

88 **INTRODUCTION**

89 SARS-CoV-2 has infected more than 600 million people and caused more than 6
90 million deaths worldwide (<https://www.worldometers.info/coronavirus>). Vaccines
91 designed primarily to elicit neutralizing antibodies against the spike (S) protein initially
92 attenuated the course of disease and protected against the development of severe
93 COVID-19 ^{1, 2, 3, 4, 5}. However, the continual emergence of viral escape variants has
94 undermined this approach, and the ongoing pandemic is now driven largely by strains
95 resistant to antibody-mediated neutralization⁶.

96
97 Several reports have indicated a likely role for SARS-CoV-2-specific T cells as a key
98 determinant of immune protection against severe COVID-19 ^{7, 8, 9, 10, 11}. More directly,
99 antigen-specific memory CD4⁺ T cells in the airways have been shown to protect mice
100 against respiratory coronaviruses after vaccination¹², and depletion studies in rhesus
101 macaques vaccinated with adenoviral-encoded S (Ad26.COVS) have implicated
102 CD8⁺ T cells as important mediators of viral control after intranasal or intratracheal
103 challenge with SARS-CoV-2¹³. It is also notable that antigen-specific memory CD4⁺ T
104 cells in the circulation have been associated with immune protection in humans after
105 influenza virus challenge ¹⁴. In line with these observations, SARS-CoV-2 has been
106 shown to induce tissue-resident memory T cell immunity^{15, 16}, but the precise correlates
107 of early viral control and disease mitigation have nonetheless remained elusive¹⁷.

108
109 In this study, we investigated the dynamics of adaptive immune responses in relation
110 to markers of disease severity during acute infection with SARS-CoV-2 in previously
111 unexposed, non-vaccinated patients. Our data provided correlative and mechanistic
112 evidence to indicate that viral nucleocapsid (NC)-specific T cells were the central
113 determinants of immune protection, limiting viral replication in the upper airways and
114 suppressing the attendant inflammatory response. Collectively, these observations
115 revealed a cellular and molecular signature of effective antiviral immunity, with
116 potential implications for the development of next-generation vaccines against COVID-
117 19.

118
119
120
121

122 **RESULTS**

123 **Viral loads in the upper airways are highly variable during acute infection with** 124 **SARS-CoV-2**

125 A total of 37 patients with acute COVID-19 were recruited into this study between May
126 and December 2020. All participants had mild symptoms that did not require
127 hospitalization (Table 1)¹⁸. Twenty-five of these patients were recruited within the first
128 week of symptom onset (median = 5 days, interquartile range [IQR] = 4–6 days). Upper
129 airways viral loads (UA-VLs) were highly variable during the first week of infection
130 (median = 1.7×10^8 RNA copies/ml, range = 1.7×10^2 to 9.8×10^{10} RNA copies/ml)
131 (Figure 1A). IgA and IgG responses against the viral S protein were below the detection
132 threshold in all cases (Supplementary Figure 1), and only 12% of donors (3/25) had
133 detectable neutralization titers at the time of recruitment (Figure 1B). In the second
134 week of infection, all patients had lower UA-VLs (median = 2.1×10^3 RNA copies/ml,
135 range = 4.8×10^0 to 1.1×10^7 RNA copies/ml) (Figure 1B), and SARS-CoV-2
136 neutralization titers became detectable in 92% of cases (23/25), subsequently peaking
137 during the third week of infection (median IC₅₀ = 165, IQR = 66–375) (Figure 1B). Most
138 subjects retained detectable neutralization titers until the last study visit 6 months after
139 symptom onset (Figure 1B). A similar pattern was observed for antibody responses
140 against the viral NC protein (Supplementary Figure 1).

141
142 Collectively, these data established that UA-VLs peaked during the first week of
143 infection, before the emergence of detectable antibody responses, and varied
144 considerably among individuals with mild COVID-19.

145 146 **Nucleocapsid-specific T cell responses correlate inversely with upper airways** 147 **viral loads during acute infection with SARS-CoV-2**

148 T cell responses against the viral NC and S proteins were measured longitudinally
149 using flow cytometry to detect the intracellular production of IFN- γ . SARS-CoV-2-
150 specific CD4⁺ T cells were detected more frequently than SARS-CoV-2-specific CD8⁺
151 T cells (Figure 2 A–E). Area under the curve (AUC) analyses revealed that the overall
152 frequency of SARS-CoV-2-specific CD4⁺ T cells was higher than the overall frequency
153 of SARS-CoV-2-specific CD8⁺ T cells per day across all time points in the study ($p <$
154 0.0001) (Figure 2F), and in both lineages, the overall frequency of NC-specific T cells
155 was higher than the overall frequency of S-specific T cells per day across all time points

156 in the study ($p = 0.0102$) (Figure 2G). Higher frequencies of NC-specific CD4⁺ T cells
157 and S-specific CD8⁺ T cells were detected in patients versus healthy controls during
158 the first week of infection ($p = 0.0005$ for NC, $p = 0.0085$ for S) (Figure 2H and I).
159 SARS-CoV-2-specific CD4⁺ T cell responses typically peaked during the third week
160 after symptom onset for NC (median = 0.045% of CD4⁺ T cells) and S (median =
161 0.023% of CD4⁺ T cells), whereas SARS-CoV-2-specific CD8⁺ T cell responses
162 typically peaked during the fourth week after symptom onset for NC (median = 0.024%
163 of CD8⁺ T cells) and during the third week after symptom onset for S (median = 0.033%
164 of CD8⁺ T cells) (Figure 2H and I). Of note, 51.1% of patients mounted detectable
165 SARS-CoV-2-specific CD4⁺ T cell responses during the first week of infection, and
166 37.7% of patients mounted detectable SARS-CoV-2-specific CD8⁺ T cell responses
167 during the first week of infection (Figure 2E).

168

169 In total, 21% of healthy controls had detectable NC-specific T cell responses, and 52%
170 of healthy controls had detectable S-specific T cell responses (Figure 2H and I),
171 consistent with previous reports^{9, 19, 20, 21}. To investigate this phenomenon, we
172 measured serological reactivity against the four common cold coronaviruses (CCCVs).
173 Strain-specific antibody responses were detected in most patients for NL63 (80%),
174 OC43 (64%), and HKU1 (68%), whereas only 48% of patients were seropositive for
175 229E (Supplementary Figure 2A). Data from healthy controls are shown in
176 Supplementary Figure 2B. There was no association between the presence of early
177 NC-specific CD4⁺ or CD8⁺ T cell responses and serological reactivity against CCCVs
178 (Supplementary Figure 2C).

179

180 In further analyses, we found a strong inverse correlation between the overall
181 frequency of circulating NC-specific T cells during the first week after symptom onset
182 and UA-VLs ($r = -0.76$, $p < 0.0001$) (Figure 3A). This association was strongest for
183 NC-specific CD4⁺ T cells ($r = -0.70$, $p < 0.0001$) but was also significant for NC-specific
184 CD8⁺ T cells ($r = -0.45$, $p = 0.02$) (Figure 3A). In contrast, we found no such
185 correlations for S-specific T cells, irrespective of lineage (Figure 3B). Using a censored
186 linear mixed effects model with random individual effects to control for other potential
187 confounders, we also found that incremental increases in the frequencies of NC-
188 specific but not S-specific CD4⁺ and CD8⁺ T cells reduced individual UA-VLs
189 (Supplementary Figure 3). Age and gender did not play a significant role. Importantly,

190 the model also controlled for time after symptom onset in the regression analysis,
191 ensuring the results were independent of any natural decay in the UA-VLs.

192

193 Collectively, these findings supported a role for early IFN- γ -expressing NC-specific
194 CD4⁺ and CD8⁺ T cells as mediators of viral clearance in the upper airways, which
195 could have important implications for the development of more effective vaccines
196 against SARS-CoV-2.

197

198 **Nucleocapsid-specific T cell responses correlate inversely with markers of** 199 **systemic inflammation during acute infection with SARS-CoV-2**

200 Excessive production of various chemokines and cytokines, including CXCL10 and
201 CXCL11, has been linked with the severity of COVID-19^{22, 23}. Using a 26-plex panel,
202 we found that plasma concentrations of CXCL10 and CXCL11 were significantly
203 elevated during the first week after symptom onset (median = 3,922 pg/ml and 97.5
204 pg/ml, respectively) compared with later time points ($p < 0.001$ or $p < 0.0001$) (Figure
205 3C, Supplementary Figure 4). Moreover, plasma concentrations of CXCL10 during the
206 first week after symptom onset correlated directly with UA-VLs ($r = 0.50$, $p = 0.01$) and
207 inversely with the frequency of circulating NC-specific T cells ($r = -0.43$, $p = 0.03$)
208 (Figure 3C). Similar correlations were found for CXCL11 ($r = 0.65$, $p = 0.0004$ versus
209 UA-VLs; $r = -0.43$, $p = 0.03$ versus NC-specific T cells) (Supplementary Figure 4).
210 Other soluble factors were also upregulated significantly in the first week after symptom
211 onset compared with later time points, including CCL3, CCL19, galectin-9, and MICA
212 (Supplementary Figure 4). Plasma concentrations of CCL2, CCL19, galectin-9, and
213 MICA correlated directly with UA-VLs ($r > 0.4$, $p < 0.05$), and plasma concentrations of
214 CCL19 and MICA correlated inversely with the frequency of circulating NC-specific T
215 cells during the first week after symptom onset ($r < -0.4$, $p < 0.05$) (Supplementary
216 Figure 4). No correlations were identified for S-specific T cells versus any analyte (data
217 not shown).

218

219 To explore the nature of these associations, we profiled the transcriptomes of
220 circulating immune cell subsets, namely CD4⁺ T cells, CD8⁺ T cells, monocytes, and
221 NK cells, isolated during the first week after symptom onset ($n = 14$ patients with mild
222 COVID-19). We initially focused our analysis on previously reported differentially
223 expressed genes (DEGs), notably *STAT1*, *OAS1*, and *PKR*, which have been

224 implicated in the clearance of SARS-CoV-1 by IFN- γ ⁺ NC-specific CD4⁺ T cells after
225 intranasal vaccination¹². In our cohort, the frequency of circulating NC-specific CD4⁺ T
226 cells correlated inversely with gene expression among circulating immune cell subsets
227 for *STAT1* (CD4⁺ T cells, $r = -0.38$, $p = 0.029$; CD8⁺ T cells, $r = -0.53$, $p = 0.001$;
228 monocytes, $r = -0.34$, $p = 0.05$; NK cells, $r = -0.39$, $p = 0.023$), *OAS1* (CD4⁺ T cells, r
229 $= -0.21$, $p = 0.25$; CD8⁺ T cells, $r = -0.47$, $p = 0.006$; monocytes, $r = -0.60$, $p = 0.0002$;
230 NK cells, $r = -0.5$, $p = 0.003$), and *PKR* (CD4⁺ T cells, $r = -0.42$, $p = 0.015$; CD8⁺ T
231 cells, $r = -0.23$, $p = 0.199$; monocytes, $r = -0.51$, $p = 0.003$; NK cells, $r = -0.43$, $p =$
232 0.012) (Figure 4A). Similar correlation trends were observed among the same immune
233 cell subsets for NC-specific CD8⁺ T cells, and direct correlations were detected for all
234 three markers versus UA-VLs (Figure 4A).

235
236 Next, we conducted mean expression analyses for pathways classified as *Signal*
237 *Transduction*, *Signaling Molecules and Interaction*, *Immune System*, and *Cell Growth*
238 *and Death according to the Kyoto Encyclopedia of Genes and Genomes (KEGG)*
239 *database*. Correlations were performed against the frequency of circulating NC-
240 specific CD4⁺ T cells (Figure 4B), the frequency of circulating NC-specific CD8⁺ T cells
241 (Figure 4C), and UA-VLs (Figure 4D). Signaling pathways involved in the host
242 response and inflammation, including those for NF- κ B, RIG-1-like receptors (RLRs),
243 and JAK-STAT, generally correlated inversely with the frequency of NC-specific CD4⁺
244 T cells and directly with UA-VLs (Figure 4B and D). The frequency of circulating NC-
245 specific CD8⁺ T cells also correlated inversely with the NF-KB pathway but directly with
246 other pathways, including those associated with cytotoxicity (Figure 4C). The pathway
247 scores were then included in the censored linear mixed effect model for further
248 investigation. These analyses confirmed that the pathway scores for NF-KB and RLR
249 signaling, as well as other pathways, including antigen processing and presentation,
250 were influenced by UA-VLs for at least one of the immune cell subsets in each pathway
251 (Supplementary Figure 5).

252
253 Unsupervised hierarchical clustering further revealed three distinct clusters within the
254 overall data set (Figure 4E). One group incorporating NC-specific CD4⁺ T cell
255 responders was characterized predominantly by downregulation of immune system
256 and signaling pathways among circulating immune cell subsets, whereas another
257 cluster incorporating NC-specific CD4⁺ T cell non-responders was characterized

258 predominantly by upregulation of immune system and signaling pathways among
259 circulating immune cell subsets (Figure 4E). The other cluster incorporated a mixed
260 group of NC-specific CD4⁺ T cell responders and non-responders, in which immune
261 system and signaling pathways among circulating immune cell subsets were either
262 upregulated, predominantly among T cells, or downregulated, predominantly among
263 monocytes and NK cells (Figure 4E).

264

265 Collectively, these data showed that systemic upregulation of inflammatory pathways
266 during early infection was positively associated with high viral burdens in the upper
267 airways and negatively associated with the frequencies of circulating NC-specific CD4⁺
268 and CD8⁺ T cells, which in turn suggested that these immune effectors likely mitigated
269 the inflammatory response via enhanced clearance of SARS-CoV-2.

270

271 **T cells in the upper airways express IFN- γ and cytotoxic effector molecules** 272 **during acute infection with SARS-CoV-2**

273 To pursue this line of investigation, which suggested a potential role for tissue-
274 recirculating and/or tissue-resident NC-specific CD4⁺ and/or CD8⁺ T cells as mediators
275 of viral control at the site of infection¹², we interrogated a public single-cell RNA
276 sequencing data set obtained from nasopharyngeal material collected from healthy
277 controls (n = 15), patients in intensive care with no recent history of COVID-19 (n = 6),
278 and patients with mild to severe COVID-19 (n = 37)²⁴. A total of 32,587 cells were
279 analyzed in the original study and annotated to 32 clusters spanning distinct identities
280 across the epithelial barrier and the immune system. Initial reclustering and
281 reannotation focused on T cell identity revealed multiple small clusters of CD4⁺ T cells
282 ($n_{\text{cells}} = 66$, $n_{\text{donors}} = 16$) and a single large cluster of CD8⁺ T cells ($n_{\text{cells}} = 310$, $n_{\text{donors}} =$
283 23). We then identified T cells expressing effector molecule-encoding mRNAs. The
284 most abundantly expressed transcripts encoded IFN- γ (CD4⁺ T cells: $n_{\text{donors}} = 7$, $f_{\text{cells}} =$
285 28% ; CD8⁺ T cells: $n_{\text{donors}} = 17$, $f_{\text{cells}} = 44\%$), followed by TNF (CD4⁺ T cells: $n_{\text{donors}} =$
286 6 , $f_{\text{cells}} = 18\%$; CD8⁺ T cells: $n_{\text{donors}} = 15$, $f_{\text{cells}} = 27\%$), FasL (CD4⁺ T cells: $n_{\text{donors}} = 4$,
287 $f_{\text{cells}} = 12\%$; CD8⁺ T cells: $n_{\text{donors}} = 14$, $f_{\text{cells}} = 20\%$), and CD40L (CD4⁺ T cells: $n_{\text{donors}} =$
288 7 , $f_{\text{cells}} = 14\%$), and less frequently by IL-2, IL-10, and IL-21 (Supplementary Figure 6).
289 We also detected transcripts encoding cytotoxic effector molecules, including perforin
290 (CD4⁺ T cells: $n_{\text{donors}} = 7$, $f_{\text{cells}} = 31\%$; CD8⁺ T cells: $n_{\text{donors}} = 20$, $f_{\text{cells}} = 39\%$) and
291 granzyme A (CD4⁺ T cells: $n_{\text{donors}} = 7$, $f_{\text{cells}} = 36\%$; CD8⁺ T cells: $n_{\text{donors}} = 15$, $f_{\text{cells}} =$

292 40%) (Supplementary Figure 6). Of note, *FASL*, *GZMA*, *GZMB*, and *PRF* were often
293 expressed coordinately among nasopharyngeal CD8⁺ T cells, and overall, *GZMA*,
294 *GZMB*, *IFNG*, and *PRF* were expressed less commonly among nasopharyngeal CD4⁺
295 and CD8⁺ T cells from healthy controls versus patients infected with SARS-CoV-2 ($p <$
296 0.05 for all comparisons, data not shown).

297

298 Collectively, these analyses showed that cytotoxic and other effector molecules were
299 expressed frequently among T cells isolated from the upper airways, especially in
300 patients with mild to severe COVID-19.

301

302 **T cell expression of IFN- γ in the upper airways is linked with antigen** 303 **presentation and viral control during acute infection with SARS-CoV-2**

304 Next, we identified responders ($n = 7$) and non-responders ($n = 9$) among the patients
305 with mild to severe COVID-19, defined as those with or without nasopharyngeal IFN-
306 γ^+ T cells, respectively. Further interrogation of the original data segregated by
307 responder status revealed that 17 of the 32 initially annotated cell subsets contained
308 DEGs (Figure 5A). The highest numbers of upregulated DEGs were present in
309 developing ($n = 291$) or IFN-responsive ciliated cells ($n = 184$) (Figure 5A,
310 Supplementary Tables 1 and 2), which are abundant in the nasopharynx and frequent
311 targets of SARS-CoV-2²⁴. In responders, these cells overexpressed master
312 transcription factors involved in antiviral immunity, such as *STAT1* and *IRF1*, and
313 genes associated with antigen processing and presentation, such as *HLA-A*, *HLA-B*,
314 *HLA-C*, *HLA-E*, *HLA-DQB1*, *B2M*, *TAP1*, *TAP2*, *TAPBP*, and the proteasome subunit
315 *PSMD6*, many of which are regulated by *IRF1* (Figure 5B, Supplementary Table 1).
316 Antigen processing and presentation gene sets were also significantly upregulated in
317 both cell types across multiple GO terms (Figure 5C, Supplementary Table 2). Similar
318 enrichments were observed for developing ciliated cells in pathway analyses aligned
319 to KEGG (Figure 5D, Supplementary Table 2). Moreover, these cells exhibited high
320 combined scores for apoptosis, cellular senescence, necroptosis, and signaling via
321 TNF (Figure 5D, Supplementary Table 2). Of further note, developing ciliated cells
322 overexpressed gene sets in responders that associated with the negative regulation of
323 translation under stress, including the PERK-mediated unfolded protein response,
324 consistent with innate suppression of viral replication after entry²⁵, and IFN-responsive

325 ciliated cells overexpressed *IFITM1*, *IFITM2*, and *IFITM3*, which encode proteins
326 known to modulate viral entry^{26, 27, 28, 29}.

327 In further analyses, we found that 54 genes were differentially upregulated among
328 nasopharyngeal CD8⁺ T cells in the presence of site-matched IFN- γ ⁺ CD4⁺ T cells,
329 most prominently those associated with the induction of apoptosis and cytotoxicity,
330 such as *GZMA*, *GZMB*, and *GZML* (Figure 5B, Supplementary Tables 1 and 2). Other
331 notable DEGs included *SELL*, which encodes L-selectin, and genes encoding multiple
332 ribosomal subunits (Figure 5B, Supplementary Table 1), which were linked in GO terms
333 with protein translation, RNA processing, and protein export/transport to the cell
334 membrane (Figure 5C, Supplementary Table 2). Some of these genes have been
335 linked previously with CD8⁺ T cell activation³⁰. In addition, we noted that many genes
336 associated with antigen processing and presentation were upregulated
337 contemporaneously, including various *HLA-A*, *HLA-B*, *HLA-C*, *B2M*, *IFI6*, and *TAP1*
338 (Figure 5C, Supplementary Tables 1 and 2). Importantly, we also found that
339 responders exhibited higher fractions of SARS-CoV-2 RNA-free cells and lower
340 abundances of SARS-CoV-2 RNA in infected cells compared with non-responders
341 (responders, $n_{\text{cells}} = 11,871$; non-responders, $n_{\text{cells}} = 5,386$; $p = 0.00013$), thereby
342 aligning our results with biological efficacy (Supplementary Figure 7).

343

344 Collectively, these findings indicated that the presence of activated T cells in the upper
345 airways was associated with enhanced target cell conditioning for immune recognition,
346 globally upregulated viral clearance mechanisms, and better localized control of
347 SARS-CoV-2.

348

349 **DISCUSSION**

350 In this study, we undertook a comprehensive evaluation of adaptive immune
351 responses, inflammatory cascades, and gene expression profiles among circulating
352 immune cell subsets to define the correlates of viral control during acute infection with
353 SARS-CoV-2. We found that genetic and plasma markers of systemic inflammation
354 peaked during the first week after symptom onset and correlated directly with UA-VLs,
355 whereas the contemporaneous frequencies of circulating viral NC-specific CD4⁺ and
356 CD8⁺ T cells correlated inversely with various inflammatory markers and UA-VLs.
357 Moreover, we identified high frequencies of activated CD4⁺ and CD8⁺ T cells in acutely
358 infected nasopharyngeal tissue, many of which expressed genes encoding various
359 effector molecules, such as cytotoxic proteins and IFN- γ . The presence of IFN- γ ⁺ T
360 cells in the infected epithelium was further linked with common patterns of gene
361 expression among virus-susceptible target cells and better local control of SARS-CoV-
362 2. Collectively, these results indicated a protective role for viral NC-specific T cells
363 during the acute phase of infection with SARS-CoV-2, thereby providing an immune
364 correlate that could inform the development of more effective vaccines against COVID-
365 19.

366
367 T cells have been implicated as mediators of immune protection in some but not all
368 studies of acute infection with SARS-CoV-2^{7, 8, 9, 11}. These discrepancies may relate to
369 the exact timing of sample acquisition. In our study, the inverse correlation between
370 circulating viral NC-specific T cell frequencies and UA-VLs was apparent only during
371 the first week after symptom onset, prior to seroconversion. At this time, many of our
372 patients exhibited high plasma concentrations of proinflammatory cytokines, many of
373 which have been linked previously with severe disease, including the CXCR3 ligand
374 CXCL10^{8, 31, 32}. In line with an earlier study⁸, we detected an inverse correlation
375 between the frequencies of circulating viral NC-specific T cells and plasma
376 concentrations of CXCL10, which in turn correlated directly with UA-VLs. Similar
377 relationships were observed for NF- κ B signaling pathway gene expression scores
378 among circulating immune cell subsets, hinting at a potential mechanism. Indeed,
379 many cytokines are transactivated via the NF- κ B signaling pathway, including those
380 implicated previously in the inflammatory storm that accompanies severe COVID-19,
381 such as IL-1, IL-6, IL-8, TNF, and CXCL10³³. These results supported the notion that
382 immune control of early viral replication attenuates the local and systemic inflammation

383 characteristic of severe COVID-19³⁴. Unexposed individuals frequently harbor cross-
384 reactive T cells with functional specificity for SARS-CoV-2, which likely arise in the
385 memory pool as consequence of previous infections with other viruses that exhibit a
386 degree of structural homology, such as CCCVs^{19, 20, 21}. In our study, all patients were
387 seropositive for one or more CCCVs before the emergence of detectable antibody
388 responses against SARS-CoV-2, and many healthy controls exhibited T cell cross-
389 reactivity against S (54%) and NC (21%). However, it should be noted that amino acid
390 sequence conservation between CCCVs and SARS-CoV-2 is rather limited across NC
391 (<30%), and that *de novo* priming of antiviral T cells from the naive pool could have
392 occurred before clinical presentation³⁵.

393

394 Analogous to our finding that viral NC-specific but not viral S-specific T cell frequencies
395 correlated inversely with UA-VLs, previous work has identified broad T cell reactivity
396 against the major viral Gag proteins (matrix, capsid, and NC) but not the viral Env
397 protein as a correlate of immune protection against HIV-1^{36, 37}. It is notable here that
398 the corresponding virions are known to contain substantially higher amounts of NC
399 compared with S or Env, respectively, and that target cells infected with SARS-CoV-2
400 *in vitro* have been shown to express approximately fivefold more NC compared with
401 S^{38, 39, 40}. High expression of NC has been reported *ex vivo* for upper airways target
402 cells infected with SARS-CoV-2²⁴. It is also notable that early viral matrix-specific and
403 NC-specific T cell responses have been associated with protection against disease
404 and reduced viral shedding after influenza virus infection¹⁴. The abundant expression
405 of internal viral proteins may therefore facilitate early antigen presentation at surface
406 densities sufficient to trigger cognate T cells more rapidly than external viral proteins,
407 leading to greater immune efficacy. This paradigm makes sense in the context of our
408 study and cautions against vaccine strategies that immunize solely against the S
409 protein of SARS-CoV-2.

410

411 IFN- γ ⁺ T cells were common in acutely infected nasopharyngeal tissue, likely as a
412 consequence of direct specificity for SARS-CoV-2. Moreover, the presence of
413 nasopharyngeal IFN- γ ⁺ T cells was associated with distinct patterns of gene
414 expression among site-matched target cells, which upregulated pathways associated
415 with antigen processing and presentation, apoptosis regulation, and innate antiviral
416 responses, and also less frequently harbored SARS-CoV-2 RNA. Contemporaneously,

417 the presence of nasopharyngeal IFN- γ ⁺ CD4⁺ T cells was associated with the
418 expression of effector genes among site-matched CD8⁺ T cells, especially those
419 associated with cytotoxicity and *SELL*, which encodes L-selectin. It is notable here that
420 L-selectin plays a critical role in transendothelial migration, which is indispensable for
421 viral clearance, at least in mice⁴¹. Transcripts encoding cytotoxic proteins were also
422 present in nasopharyngeal CD4⁺ T cells, indicating direct lytic activity^{14, 42, 43}. In line
423 with these findings, which suggested a coordinated network of viral suppression
424 mechanisms driven by the influx of IFN- γ ⁺ T cells during acute infection,
425 nasopharyngeal target cells also expressed lower amounts of SARS-CoV-2 RNA.

426
427 Several preclinical studies have provided support for the notion that next-generation
428 vaccines would benefit from the inclusion of NC antigens to enhance immune efficacy
429 against SARS-CoV-2. For example, IFN- γ production by viral NC-specific T cells in the
430 airways was found to be a key determinant of outcome in mice infected with influenza
431 virus or SARS-CoV-1^{12, 43}, and local immunization with a single conserved NC epitope
432 recognized by CD4⁺ T cells was sufficient to protect mice from MERS or SARS-CoV-
433 1¹². Intranasal vaccination of cynomolgus macaques with structural proteins from the
434 inner virion core has also been shown to induce potent NC-specific T cell immunity and
435 reduce peak UA-VLs by almost two orders of magnitude in the absence of neutralizing
436 antibody responses against SARS-CoV-2⁴⁴. Moreover, convalescent patients have
437 been shown to harbor tissue-resident memory T cells targeting the most immunogenic
438 regions of SARS-CoV-2, including epitopes derived from NC¹⁶, consistent with a role
439 in protection against recurrent episodes of COVID-19^{45, 46}.

440
441 There are several limitations to our study. First, our cohort was relatively small and did
442 not include patients with severe COVID-19. Second, we only report correlations,
443 precluding a definitive assessment of antiviral efficacy. Third, we were unable to define
444 antigen specificity in the single-cell RNA sequencing data set, instead relying on the
445 expression of IFN- γ mRNA as a surrogate marker of T cell activation driven by cognate
446 engagement with epitopes derived from SARS-CoV-2⁴⁷. Fourth, overlapping peptide
447 sets can be suboptimal for the detection of functional CD8⁺ T cell responses, albeit
448 with the concomitant advantage of global antigenic coverage^{36, 48}. In spite of these
449 caveats, our results provided clear evidence of a protective role for viral NC-specific T
450 cells in the context of acute infection with SARS-CoV-2, thereby arguing for inclusion

451 of the corresponding antigens in next-generation vaccines designed to combat COVID-
452 19.

453

454

455

456

457

458

459

460

461

462

463

464

465

466

467

468

469

470

471

472

473

474

475

476

477

478

479

480

481

482

483 **Acknowledgments**

484 We wholeheartedly thank all study participants for their time, patience, trust and their
485 constancy. We are grateful for the financial support of the Bavarian State Ministry of
486 Science and the Arts (KoCo19), from the Deutsche Forschungsgemeinschaft,
487 Germany (reference number: GE 2128/3-1 and HO 2228/12-1), from the Bavarian
488 State Ministry of Science and the Arts, Germany (Project Langfristige Nachverfolgung
489 der zellulären und humoralen Immunantwort nach SARS-CoV-2-Infektion und Impfung
490 2021) and from the Ministry for Education and Research, Germany (proj. nr.:
491 01KI20271). Euroimmun, Roche and Mikrogen, provided kits and machines for
492 analyses at discounted rates. This study would not have been possible without the
493 passionate contribution of the staff of the Division of Infectious Diseases and Tropical
494 Medicine at the University Hospital, LMU Munich, as well as all medical students
495 involved in the field work. Part of this work has been done for the doctoral thesis of
496 TME, KP, MHU and FD.

497
498 Members of the KoCo19 study group: Mohamed Ibraheem Mohamed Ahmed, Emad
499 Alamoudi, Jared Anderson, Maximilian Baumann, Marc Becker, Marieke Behlen,
500 Jessica Beyerl, Rebecca Böhnlein, Isabel Brand, Anna Brauer, Vera Britz, Jan Brugger,
501 Friedrich Caroli, Lorenzo Contento, Max Diefenbach, Jana Diekmannshemke, Paulina
502 Diepers, Anna Do, Gerhard Dobler, Jürgen Durner, Ute Eberle, Judith Eckstein, Tabea
503 Eser, Volker Fingerle, Jonathan Frese, Felix Forster, Turid Frahnnow, Günter Fröschl,
504 Christiane Fuchs, Mercè Garí, Otto Geisenberger, Leonard Gilberg, Kristina Gillig,
505 Philipp Girl, Arlett Heiber, Christian Hinske, Janna Hoefflin, Tim Hofberger, Michael
506 Höfingler, Larissa Hofmann, Sacha Horn, Kristina Huber, Christian Janke, Ursula
507 Kappl, Charlotte Kiani, Arne Kroidl, Michael Laxy, Ronan Le Gleut, Reiner Leidl, Felix
508 Lindner, Silke Martin, Rebecca Mayrhofer, Anna-Maria Mekota, Hannah Müller,
509 Katharina Müller, Dafni Metaxa, Leonie Pattard, Michel Pletschette, Michael Pritsch,
510 Stephan Prückner, Konstantin Pusl, Peter Pütz, Ernst-Markus Quenzel, Katja Radon,
511 Elba Raimúndez, Camila Rothe, Nicole Schäfer, Yannik Schälte, Paul Schandelmaier,
512 Lara Schneider, Sophie Schultz, Mirjam Schunk, Lars Schwettmann, Heidi Seibold,
513 Peter Sothmann, Paul Stapor, Fabian Theis, Verena Thiel, Sophie Thiesbrummel,
514 Niklas Thur, Julia Waibel, Claudia Wallrauch, Franz Weinauer, Simon Winter, Julia

515 Wolff, Pia Wullinger, Houda Yaqine, Sabine Zange, Eleftheria Zeggini, Thomas
516 Zimmermann, Anna Zielke.

517

518 **AUTHOR CONTRIBUTIONS**

519 TME performed most of the experiments and analyzed data supported by MIMA, FD,
520 KH, KP, RRA, NC, and AW; OB, KP, AL, and LN analyzed data; MHu and JH
521 performed computational modeling; KH and LL performed HLA typing; GP performed
522 viral sequencing; MB and DAP provided intellectual input; JR, PK, AM, LO, IK, and
523 MHo contributed samples; KV and FK measured neutralizing antibodies; LO, AW, IK,
524 MHo, and CG conceived the study and wrote the clinical protocol; JH, MHo, and CG
525 acquired funding; TME, OB, and CG wrote the manuscript with input from all
526 contributors.

527

528 **DECLARATION OF INTERESTS**

529 The authors have no competing interests to declare.

530

531

532 **TABLES**

533

534 **Table 1. Patient characteristics.**

535

Patients	37
Gender (female)	20 [54.5%]
Median age (years) [IQR]	36 [30/49.5]
WHO score 1	1 [2.7%]
WHO score 2	14 [37.8%]
WHO score 3	22 [59.5%]
Lung involvement	21 [56.75%]
Recruited within first week after symptom onset	25 [67.75%]
Neutralizing antibodies (1–7 days after symptom onset)	4 [16%]
Anti-Ig nucleocapsid (1–7 days after symptom onset)	2 [7.6%]
Anti-IgA spike (1–7 days after symptom onset)	0
Anti-IgG spike (1–7 days after symptom onset)	0
Median log UA-VL (1–7 days after symptom onset) [IQR]	8.2 [6.9/8.8]
Median log UA-VL (8–14 days after symptom onset) [IQR]	3.3 [1.7/5.03]

536

537 IQR, interquartile range; UA-VL, upper airways viral load (RNA copies/ml).

538 **MATERIALS AND METHODS**

539

540 **Study participants**

541 A total of 37 patients with acute COVID-19 were recruited into this study between May
542 and December 2020 under the umbrella of the longitudinal KoCo19 Study⁴⁹. All
543 participants tested positive for SARS-CoV-2 via RT-PCR. At the time of recruitment,
544 only the Wuhan strain (lineage A) was circulating in Germany. Clinical presentation
545 was assessed using WHO Clinical Progression Scale. All patients in this study had
546 mild symptoms that did not require hospitalization and therefore scored a maximum of
547 3¹⁸. Healthy controls were recruited prior to vaccination and tested negative for SARS-
548 CoV-2 via RT-PCR. Written informed consent was obtained from all participants in
549 accordance with the principles of the Declaration of Helsinki. This study was approved
550 by the Ethics Committee of the Faculty of Medicine at LMU Munich (20–371).

551

552 **Upper airways viral loads**

553 Nasopharyngeal viral loads were quantified as described previously⁴⁹. Briefly, RT-PCR
554 was performed using a TANBead Maelstrom 9600 (Taiwan Advanced Nanotech Inc.)
555 with an OptiPure Viral Auto Plate Kit (Taiwan Advanced Nanotech Inc.). SARS-CoV-2
556 RNA was quantified using an Allplex 209-nCov Assay (SeeGene) with a STARlet IVD
557 (SeeGene). UA-VLs were calculated using standardized dilutions of SARS-CoV-2 RNA
558 (INSTAND).

559

560 **Antibody titers**

561 SARS-CoV-2-specific antibodies were assayed in EDTA plasma as described
562 previously^{50, 51} using the following kits: Anti-SARS-CoV-2-ELISA Anti-S1 IgA (EI-S1-
563 IgA, Euroimmun), Anti-SARS-CoV-2-ELISA Anti-S1 IgG (EI-S1-IgG, Euroimmun), and
564 Elecsys Anti-SARS-CoV-2 Anti-N (Ro-N-Ig, Roche).

565

566 **Neutralization assays**

567 Pseudotyped viral particles were generated via cotransfection of HEK 293T cells with
568 plasmids encoding HIV-1 Tat, HIV-1 Gag/Pol, HIV-1 Rev, luciferase, and the S protein
569 of SARS-CoV-2 (Wu01 S, EPI_ISL_406716 lacking the cytoplasmic domain) using the
570 FuGENE 6 Transfection Reagent (Promega). Culture supernatants were harvested at
571 48 h and 72 h after transfection, passed through a filter (pore size = 0.45 µm), and

572 stored at -80°C . Viral titers were established by infecting ACE2-expressing 293 T
573 cells as described previously⁵². Luciferase activity was revealed after 48 h via the
574 addition of luciferin/lysis buffer (10 mM MgCl_2 , 0.3 mM ATP, 0.5 mM coenzyme A, 17
575 mM IGEPAL, and 1 mM D-luciferin in Tris-HCL) and measured using a Tristar
576 Microplate Reader (Berthold Technologies). Neutralization assays were performed
577 using serum samples as described previously⁵³(Vanshylla *et al.*, 2021). Briefly, serial
578 dilutions of serum were incubated with pseudovirus supernatants for 1 h at 37°C .
579 ACE2-expressing 293 T cells were then added in 15 $\mu\text{g}/\text{ml}$ polybrene and incubated
580 for a further 48 h at 37°C . Luciferase activity was determined as above. Results were
581 expressed for each sample as the 50% inhibitory dilution (ID_{50}) after subtraction of
582 background relative light units (RLUs). ID_{50} values were calculated using a non-linear
583 fit model to plot agonist versus normalized dose-response curves with variable slopes
584 in Prism version 7 (GraphPad). Samples that did not achieve 50% neutralization
585 (serum $\text{ID}_{50} = <10$) were assigned a value halfway below the lower limit of quantification
586 (serum $\text{ID}_{50} = 5$).

587

588 **Common cold coronavirus serology**

589 Antibodies against the common cold coronaviruses 229E, NL63, OC43, and HKU1
590 were assayed in CPDA plasma using a recomLine SARS-CoV-2 IgG Kit (Mikrogen
591 Diagnostik).

592

593 **Flow cytometry**

594 PBMCs were isolated within 6 h of blood collection via density gradient centrifugation
595 (Cytiva Sweden AB) and stimulated immediately with peptide pools representing the
596 NC or S proteins of SARS-CoV-2 (1 $\mu\text{g}/\text{ml}/\text{peptide}$, Miltenyi Biotec) for 16 h at 37°C
597 in the presence of anti-CD28 (clone L293, 1 $\mu\text{g}/\text{ml}$, BD Biosciences), anti-CD49d
598 (clone L25, 1 $\mu\text{g}/\text{ml}$, BD Biosciences), and brefeldin A (5 $\mu\text{g}/\text{ml}$, Sigma-Aldrich).
599 Negative control wells lacked stimulants (medium alone), and positive control wells
600 contained staphylococcal enterotoxin B (SEB, 0.6 $\mu\text{g}/\text{ml}$, Sigma-Aldrich). Cells were
601 then stained with anti-CD4–ECD (clone SFC112T4D11, Beckman Coulter), anti-CD8–
602 APC-AF750 (clone B9.11, Beckman Coulter), anti-CD57–APC (clone HNK-1,
603 BioLegend), anti-PD1–PE-Cy5.5 (clone NAT105, BioLegend), and anti-CXCR5–PE-
604 Cy7 (clone J252D4, BioLegend). Labeled cells were fixed/permeabilized using a
605 FoxP3 / Transcription Factor Staining Buffer Set (eBioscience) and further stained

606 intracellularly with anti-CD3–APC-AF700 (clone UCHT1, Beckman Coulter), anti-IFN-
607 γ –FITC (clone 4S.B3, BioLegend), anti-IL2–PE (clone MQ1-17H12, BioLegend), anti-
608 TNF- α –BV510 (clone mAb11, BioLegend), anti-CTLA-4–BV421 (clone BNI3,
609 BioLegend), anti-Ki-67–BV605 (clone Ki-67, BioLegend), and anti-CD40L–BV785
610 (clone 24-31, BioLegend). Samples were acquired using a CytoFLEX Flow Cytometer
611 (Beckman Coulter). Data analysis was performed using FlowJo software version 10
612 (FlowJo LLC). SARS-CoV-2-specific T cell responses were defined on the basis of
613 IFN- γ production and were considered positive at a frequency of $\geq 0.01\%$ after
614 background subtraction if greater than the corresponding unstimulated values by a
615 factor of ≥ 2 .

616

617 **Plasma cytokines and proteins**

618 Concentrations of CCL2, CCL3, CCL4, CCL5, CCL17, CCL19, CD23, CXCL1, CXCL4,
619 CXCL5, CXCL10, CXCL11, galectin-1, galectin-3, galectin-9, Gas6, ICAM-1, IL-2, IL-
620 4, IL-10, IL-19, MICA, NCAM-1, PD-L1, syndecan-1, and TFPI were determined in
621 CPDA plasma using a customized 26-plex marker panel (R&D Systems) as described
622 previously⁵⁴.

623

624 **RNA sequencing**

625 RNA isolation and sequencing was performed as described previously (Pekayvaz et
626 al., 2022). Briefly, libraries were prepared from immune cell subsets (n = 500 cells
627 each) using the Prime-seq protocol⁵⁵, and quality was determined using a High
628 Sensitivity DNA Kit (Agilent Bioanalyzer). Paired-end sequencing (150 bp) was
629 performed using an S1 or an S4 flow cell on a NovaSeq System (Illumina). An average
630 of $\approx 1 \times 10^7$ reads were acquired per subset per sample. Preprocessing and
631 quantification of the raw data was conducted using zUMIs⁵⁶ and referenced against
632 GENCODE V35. Further analyses were performed using non-normalized outputs that
633 mapped to exonic regions only (full data). Raw inputs were normalized using DESeq2
634 version 1.36.0⁵⁷. Analyses were limited to participants in the KoCo19 study enrolled
635 within the first week of symptom onset (n = 14) and healthy controls (n = 8). Initial
636 pathway enrichment analyses were performed using R package gage version 2.46.0⁵⁸.
637 Pathways were included from the KEGG database mapped to BRITE terms in the
638 groups *Signal Transduction* and *Signaling Molecules and Interaction* (environmental
639 information processing), *Immune System* (organismal systems), and *Cell Growth and*

640 *Death* (cellular processing). ENSEMBL IDs were used in the original data set and
641 converted to Entrez IDs using the org.Hs.eg.db R package version 3.15.0⁵⁹. ID
642 mappings for some genes were non-existent or not unique. The relevant genes were
643 discarded in the former case or assigned to the first match in the latter case.
644 Spearman's formula was used to calculate correlations among gene/pathway
645 expression, cell type frequencies, and UA-VLs. Normalized read counts were used for
646 individual genes, and average expression of composite genes was used for pathways.
647 A confidence interval was calculated using bootstrapping of the original data by
648 random resampling with replacement to estimate the range of possible correlations,
649 with subsequent calculation of the mean expression score for each relevant pathway.
650 Reference pathways were generated from 30 (smallest size) or 300 random genes
651 (biggest size). Bootstrapping was performed over 1,000 iterations for each pathway.
652 Correlation coefficients were then ordered and used to pick intervals at quantile values
653 of 2.5% (low) and 97.5% (high).

654

655 **Statistics**

656 Basic statistical analyses were performed using non-parametric tests in Prism version
657 8 (GraphPad).

658

659 **Analysis of single-cell RNA sequencing data**

660 Single-cell data from nasopharyngeal samples were acquired from the Single Cell
661 Portal (https://singlecell.broadinstitute.org/single_cell/study/SCP1289/). Data were
662 normalized using Seurat version 4.1.0⁶⁰ with Harmony version 0.1.0⁶¹ and
663 subsequently reclustered using the default settings in FindNeighbors and FindClusters.
664 One patient was excluded due to the presence of abnormally high numbers of
665 macrophages (patient 19). Characterization was performed using scCATCH version
666 3.0⁶². T cells were extracted and reclustered separately. The optimal partition was
667 determined using the silhouette function in Cluster version 2.1.3
668 (<https://guix.gnu.org/en/packages/r-cluster-2.1.3/>). Clusters were then classified again
669 using scCATCH with subset markers defined according to the Cell Marker Database⁶³.
670 One cluster was excluded on the basis of annotation failure. T cells with at least one
671 RNA read mapping to a selected function were classified as function-positive.
672 Differentially expressed genes and pathways in the IFN- γ^+ and IFN- γ^- patient groups
673 were identified using the FindMarkers function with default settings in Seurat version

674 4.1.0. Each previously reported cluster in the original annotation²⁴. was interrogated
675 with no initial cutoff for limit fold-change (LFC). All remaining clusters were used as
676 reference. CD8⁺ T cells were also identified and analyzed independently. In this case,
677 group assignments (IFN- γ ⁺ versus IFN- γ ⁻) were based on CD4⁺ T cells alone, which
678 were used for reference. Pathway and GO term analyses were based on marker genes
679 with a LFC of 0.25 in either direction and a p-value of <0.01, except for CD8⁺ T cells,
680 which occurred in low numbers and were analyzed using a p-value of <0.05.
681 Enrichment analyses were performed using enrichR (Kuleshov et al., 2016). Pathway
682 analyses were performed for *Signal Transduction*, *Signaling Molecules and Interaction*,
683 *Immune System*, and *Cell Growth and Death*. The common logarithm of SARS-CoV-2
684 total corrected RNA reported previously ²⁴ was used to quantify host cell VLs. Patient
685 groups were assigned as above. Values from all cells in the IFN- γ ⁺ and IFN- γ ⁻ groups
686 formed the test distribution for the IFN- γ ⁺ and IFN- γ ⁻ groups, and comparisons were
687 performed using a two-sided Man-Whitney U test. Similar results were obtained using
688 uncorrected read counts for SARS-CoV-2 RNA.

689

690 **Interaction models**

691 A univariate linear mixed effects model was established using the default settings in
692 CensReg⁶⁴. Point estimates for the model parameters were obtained by minimizing the
693 negative log-likelihood function using numerical minimization. Standard errors were derived
694 from the inverse of the Hessian matrix evaluated at the point estimates. The likelihood function
695 was constructed using truncated conditional normal distributions based on normality
696 assumptions about individual effects and error terms to account for the limits of viral detection.
697 A mixed effects model was also used to solidify the observed relationship as a correlation
698 between a score for the subset of pathways and cell fractions and/or VLs. A second mixed
699 model equation was added using Julia for joint modeling of subsets and VLs. This model
700 included VL as a mediator of additional confounders to evaluate the influence of the true non-
701 censored VL on each pathway score, despite the censored structure of the observed VLs. The
702 outer marginalization of random effects within the likelihood was approximated using Gauss-
703 Hermite quadrature⁶⁵, with weights obtained via the Julia package FastGaussQuadrature
704 across 10 quadrature points
705 (<https://juliaapproximation.github.io/FastGaussQuadrature.jl/stable/>). Gradients were obtained
706 using automatic differentiation in the Julia package ForwardDiff ⁶⁶. Pathways were prefiltered
707 by running ordinary least squares regressions to determine those potentially influenced by the
708 VL. Data preprocessing was conducted in Python using Pandas⁶⁷ and Numpy⁶⁸. All code is
709 publicly available at https://github.com/manuhuth/early_t_cell_control.git.

710 **LIST OF SUPPLEMENTARY TABLES**

711

712 **Supplementary Table 1. Differentially expressed genes among nasopharyngeal**
713 **ciliated cells and CD8⁺ T cells from patients with COVID-19.**

714

715 **Supplementary Table 2. Gene ontology and pathway analyses for differentially**
716 **expressed genes among nasopharyngeal ciliated cells and CD8⁺ T cells from**
717 **patients with COVID-19.**

718

719

720

721

722

723

724

725

726

727

728

729

730

731

732

733

734

735

736

737

738

739

740

741

742

743

- 744 1. Baden, L.R. *et al.* Efficacy and Safety of the mRNA-1273 SARS-CoV-2 Vaccine. *New*
745 *England Journal of Medicine* **384**, 403-416 (2020).
746
- 747 2. Polack, F.P. *et al.* Safety and Efficacy of the BNT162b2 mRNA Covid-19 Vaccine. *New*
748 *England Journal of Medicine* **383**, 2603-2615 (2020).
749
- 750 3. Gilbert, P.B. *et al.* Immune Correlates Analysis of the mRNA-1273 COVID-19 Vaccine
751 Efficacy Trial. *medRxiv* (2021).
752
- 753 4. Sadoff, J. *et al.* Final Analysis of Efficacy and Safety of Single-Dose Ad26.COV2.S. *New*
754 *England Journal of Medicine* **386**, 847-860 (2022).
755
- 756 5. Voysey, M. *et al.* Safety and efficacy of the ChAdOx1 nCoV-19 vaccine (AZD1222)
757 against SARS-CoV-2: an interim analysis of four randomised controlled trials in Brazil,
758 South Africa, and the UK. *Lancet* **397**, 99-111 (2021).
759
- 760 6. Harvey, W.T. *et al.* SARS-CoV-2 variants, spike mutations and immune escape. *Nature*
761 *Reviews Microbiology* **19**, 409-424 (2021).
762
- 763 7. Le Bert, N. *et al.* Highly functional virus-specific cellular immune response in
764 asymptomatic SARS-CoV-2 infection. *J Exp Med* **218** (2021).
765
- 766 8. Moderbacher, C.R. *et al.* Antigen-specific adaptive immunity to SARS-CoV-2 in acute
767 COVID-19 and associations with age and disease severity. *Cell* **183**, 996-1012. e1019
768 (2020).
769
- 770 9. Sekine, T. *et al.* Robust T Cell Immunity in Convalescent Individuals with
771 Asymptomatic or Mild COVID-19. *Cell* **183**, 158-168.e114 (2020).
772
- 773 10. Peng, Y. *et al.* An immunodominant NP105–113-B*07:02 cytotoxic T cell response
774 controls viral replication and is associated with less severe COVID-19 disease. *Nature*
775 *Immunology* **23**, 50-61 (2022).
776
- 777 11. Notarbartolo, S. *et al.* Integrated longitudinal immunophenotypic, transcriptional,
778 and repertoire analyses delineate immune responses in patients with COVID-19.
779 *Science Immunology* **6**, eabg5021 (2021).

780

781 12. Zhao, J. *et al.* Airway memory CD4+ T cells mediate protective immunity against
782 emerging respiratory coronaviruses. *Immunity* **44**, 1379-1391 (2016).

783

784 13. Liu, J. *et al.* CD8 T Cells Contribute to Vaccine Protection Against SARS-CoV-2 in
785 Macaques. *Science Immunology*, eabq7647 (2022).

786

787 14. Wilkinson, T.M. *et al.* Preexisting influenza-specific CD4+ T cells correlate with
788 disease protection against influenza challenge in humans. *Nat Med* **18**, 274-280
789 (2012).

790

791 15. Lim, J.M.E. *et al.* SARS-CoV-2 breakthrough infection in vaccinees induces virus-
792 specific nasal-resident CD8+ and CD4+ T cells of broad specificity. *Journal of*
793 *Experimental Medicine* **219** (2022).

794

795 16. Poon, M.M.L. *et al.* SARS-CoV-2 infection generates tissue-localized immunological
796 memory in humans. *Sci Immunol* **6**, eabl9105 (2021).

797

798 17. Kingstad-Bakke, B. *et al.* Vaccine-induced systemic and mucosal T cell immunity to
799 SARS-CoV-2 viral variants. *Proceedings of the National Academy of Sciences* **119**,
800 e2118312119 (2022).

801

802 18. Marshall, J.C. *et al.* A minimal common outcome measure set for COVID-19 clinical
803 research. *The Lancet Infectious Diseases* **20**, e192-e197 (2020).

804

805 19. Braun, J. *et al.* SARS-CoV-2-reactive T cells in healthy donors and patients with
806 COVID-19. *Nature* **587**, 270-274 (2020).

807

808 20. Lineburg, K.E. *et al.* CD8(+) T cells specific for an immunodominant SARS-CoV-2
809 nucleocapsid epitope cross-react with selective seasonal coronaviruses. *Immunity* **54**,
810 1055-1065.e1055 (2021).

811

812 21. Niessl, J. *et al.* Identification of resident memory CD8(+) T cells with functional
813 specificity for SARS-CoV-2 in unexposed oropharyngeal lymphoid tissue. *Sci Immunol*
814 **6**, eabk0894 (2021).

815

- 816 22. Buitrago-Garcia, D. *et al.* Occurrence and transmission potential of asymptomatic and
817 presymptomatic SARS-CoV-2 infections: Update of a living systematic review and
818 meta-analysis. *PLOS Medicine* **19**, e1003987 (2022).
819
- 820 23. Montazersaheb, S. *et al.* COVID-19 infection: an overview on cytokine storm and
821 related interventions. *Virology Journal* **19**, 92 (2022).
822
- 823 24. Ziegler, C.G. *et al.* Impaired local intrinsic immunity to SARS-CoV-2 infection in severe
824 COVID-19. *Cell* **184**, 4713-4733. e4722 (2021).
825
- 826 25. Zhang, L. & Wang, A. Virus-induced ER stress and the unfolded protein response.
827 *Front Plant Sci* **3**, 293 (2012).
828
- 829 26. Feeley, E.M. *et al.* IFITM3 inhibits influenza A virus infection by preventing cytosolic
830 entry. *PLoS Pathog* **7**, e1002337 (2011).
831
- 832 27. Prelli Bozzo, C. *et al.* IFITM proteins promote SARS-CoV-2 infection and are targets for
833 virus inhibition in vitro. *Nat Commun* **12**, 4584 (2021).
834
- 835 28. Tartour, K. *et al.* IFITM proteins are incorporated onto HIV-1 virion particles and
836 negatively imprint their infectivity. *Retrovirology* **11**, 103 (2014).
837
- 838 29. Zhao, X. *et al.* Interferon induction of IFITM proteins promotes infection by human
839 coronavirus OC43. *Proceedings of the National Academy of Sciences* **111**, 6756-6761
840 (2014).
841
- 842 30. Araki, K. *et al.* Translation is actively regulated during the differentiation of CD8(+)
843 effector T cells. *Nat Immunol* **18**, 1046-1057 (2017).
844
- 845 31. Delorey, T.M. *et al.* COVID-19 tissue atlases reveal SARS-CoV-2 pathology and cellular
846 targets. *Nature* **595**, 107-113 (2021).
847
- 848 32. Lucas, C. *et al.* Longitudinal analyses reveal immunological misfiring in severe COVID-
849 19. *Nature* **584**, 463-469 (2020).
850

- 851 33. Blanco-Melo, D. *et al.* Imbalanced Host Response to SARS-CoV-2 Drives Development
852 of COVID-19. *Cell* **181**, 1036-1045.e1039 (2020).
853
- 854 34. Rendeiro, A.F. *et al.* The spatial landscape of lung pathology during COVID-19
855 progression. *Nature* **593**, 564-569 (2021).
856
- 857 35. Nelson, C.E. *et al.* Mild SARS-CoV-2 infection in rhesus macaques is associated with
858 viral control prior to antigen-specific T cell responses in tissues. *Sci Immunol*,
859 eabo0535 (2022).
860
- 861 36. Geldmacher, C. *et al.* In a mixed subtype epidemic, the HIV-1 Gag-specific T-cell
862 response is biased towards the infecting subtype. *AIDS* **21**, 135-143 (2007).
863
- 864 37. Kiepiela, P. *et al.* CD8+ T-cell responses to different HIV proteins have discordant
865 associations with viral load. *Nature medicine* **13**, 46-53 (2007).
866
- 867 38. Bojkova, D. *et al.* Proteomics of SARS-CoV-2-infected host cells reveals therapy
868 targets. *Nature* **583**, 469-472 (2020).
869
- 870 39. Briggs, J.A. *et al.* The stoichiometry of Gag protein in HIV-1. *Nat Struct Mol Biol* **11**,
871 672-675 (2004).
872
- 873 40. Zhu, P. *et al.* Electron tomography analysis of envelope glycoprotein trimers on HIV
874 and simian immunodeficiency virus virions. *Proc Natl Acad Sci U S A* **100**, 15812-
875 15817 (2003).
876
- 877 41. Mohammed, R.N. *et al.* L-selectin Is Essential for Delivery of Activated CD8(+) T Cells
878 to Virus-Infected Organs for Protective Immunity. *Cell Rep* **14**, 760-771 (2016).
879
- 880 42. Casazza, J.P. *et al.* Acquisition of direct antiviral effector functions by CMV-specific
881 CD4+ T lymphocytes with cellular maturation. *J Exp Med* **203**, 2865-2877 (2006).
882
- 883 43. Teijaro, J.R., Verhoeven, D., Page, C.A., Turner, D. & Farber, D.L. Memory CD4 T cells
884 direct protective responses to influenza virus in the lungs through helper-
885 independent mechanisms. *J Virol* **84**, 9217-9226 (2010).
886

- 887 44. Ishii, H. *et al.* Neutralizing-antibody-independent SARS-CoV-2 control correlated with
888 intranasal-vaccine-induced CD8(+) T cell responses. *Cell Rep Med* **3**, 100520 (2022).
889
- 890 45. Gazit, S. *et al.* SARS-CoV-2 Naturally Acquired Immunity vs. Vaccine-induced
891 Immunity, Reinfections versus Breakthrough Infections: a Retrospective Cohort
892 Study. *Clin Infect Dis* (2022).
893
- 894 46. Yu, E.D. *et al.* Development of a T cell-based immunodiagnostic system to
895 effectively distinguish SARS-CoV-2 infection and COVID-19 vaccination status. *Cell*
896 *Host & Microbe* **30**, 388-399.e383 (2022).
897
- 898 47. Fischer, D.S. *et al.* Single-cell RNA sequencing reveals ex vivo signatures of SARS-CoV-
899 2-reactive T cells through 'reverse phenotyping'. *Nature Communications* **12**, 4515
900 (2021).
901
- 902 48. Draenert, R. *et al.* Constraints on HIV-1 evolution and immunodominance revealed in
903 monozygotic adult twins infected with the same virus. *J Exp Med* **203**, 529-539
904 (2006).
905
- 906 49. Puchinger, K. *et al.* The interplay of viral loads, clinical presentation, and serological
907 responses in SARS-CoV-2—Results from a prospective cohort of outpatient COVID-19
908 cases. *Virology* (2022).
909
- 910 50. Radon, K. *et al.* From first to second wave: follow-up of the prospective COVID-19
911 cohort (KoCo19) in Munich (Germany). *BMC Infect Dis* **21**, 925 (2021).
912
- 913 51. Pritsch, M. *et al.* Prevalence and Risk Factors of Infection in the Representative
914 COVID-19 Cohort Munich. *Int J Environ Res Public Health* **18** (2021).
915
- 916 52. Crawford, K.H.D. *et al.* Protocol and Reagents for Pseudotyping Lentiviral Particles
917 with SARS-CoV-2 Spike Protein for Neutralization Assays. *Viruses* **12** (2020).
918
- 919 53. Vanshylla, K. *et al.* Kinetics and correlates of the neutralizing antibody response to
920 SARS-CoV-2 infection in humans. *Cell Host Microbe* **29**, 917-929.e914 (2021).
921

- 922 54. Muefong, C.N. *et al.* Major Neutrophil-Derived Soluble Mediators Associate With
923 Baseline Lung Pathology and Post-Treatment Recovery in Tuberculosis Patients. *Front*
924 *Immunol* **12**, 740933 (2021).
925
- 926 55. Janjic, A. *et al.* Prime-seq, efficient and powerful bulk RNA sequencing. *Genome*
927 *biology* **23**, 1-27 (2022).
928
- 929 56. Parekh, S., Ziegenhain, C., Vieth, B., Enard, W. & Hellmann, I. zUMIs - A fast and
930 flexible pipeline to process RNA sequencing data with UMIs. *Gigascience* **7** (2018).
931
- 932 57. Love, M.I., Huber, W. & Anders, S. Moderated estimation of fold change and
933 dispersion for RNA-seq data with DESeq2. *Genome Biology* **15**, 550 (2014).
934
- 935 58. Luo, W., Friedman, M.S., Shedden, K., Hankenson, K.D. & Woolf, P.J. GAGE: generally
936 applicable gene set enrichment for pathway analysis. *BMC bioinformatics* **10**, 1-17
937 (2009).
938
- 939 59. Carlson, M. org. hs. eg. db: Genome wide annotation for human. R package version
940 3.8. 2, 10.18129/B9. *BIOC. ORG. HS. EG. DB* (2019).
941
- 942 60. Hao, Y. *et al.* Integrated analysis of multimodal single-cell data. *Cell* **184**, 3573-
943 3587.e3529 (2021).
944
- 945 61. Korsunsky, I. *et al.* Fast, sensitive and accurate integration of single-cell data with
946 Harmony. *Nature Methods* **16**, 1289-1296 (2019).
947
- 948 62. Shao, X. *et al.* scCATCH: Automatic Annotation on Cell Types of Clusters from Single-
949 Cell RNA Sequencing Data. *iScience* **23**, 100882 (2020).
950
- 951 63. Zhang, X. *et al.* CellMarker: a manually curated resource of cell markers in human and
952 mouse. *Nucleic Acids Research* **47**, D721-D728 (2018).
953
- 954 64. Henningsen, A. Estimating censored regression models in R using the censReg
955 Package. *R package vignettes* **5**, 12 (2010).
956

- 957 65. Steen, N., Byrne, G. & Gelbard, E. Gaussian Quadratures for the Integrals $\int_0^\infty e^{-x^2} f(x) dx$ and $\int_0^b e^{-x^2} f(x) dx$. *Mathematics of Computation*, 661-671 (1969).
958
959
- 960 66. Revels, J., Lubin, M. & Papamarkou, T. Forward-mode automatic differentiation in
961 Julia. *arXiv preprint arXiv:1607.07892* (2016).
962
- 963 67. McKinney, W. Data structures for statistical computing in python. Proceedings of the
964 9th Python in Science Conference; 2010: Austin, TX; 2010. p. 51-56.
965
- 966 68. Harris, C.R. *et al.* Array programming with NumPy. *Nature* **585**, 357-362 (2020).
967
968

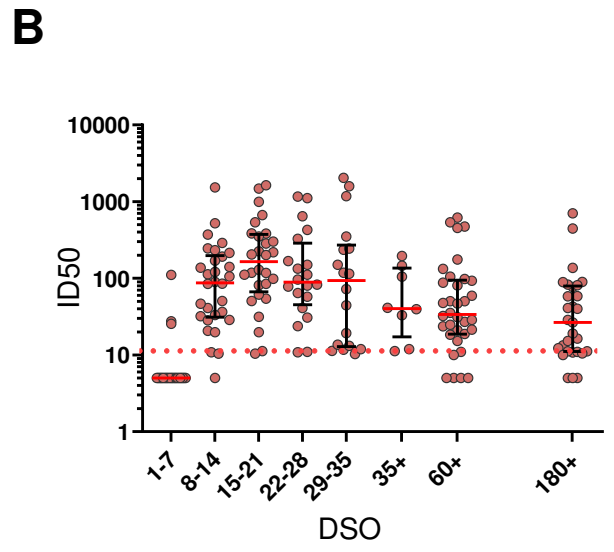
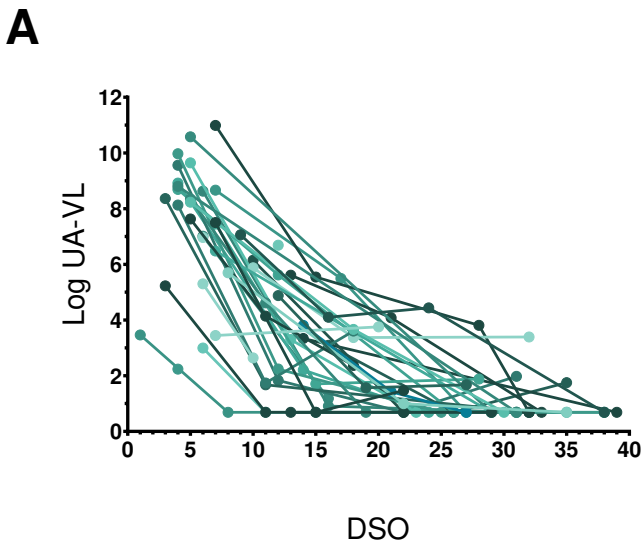
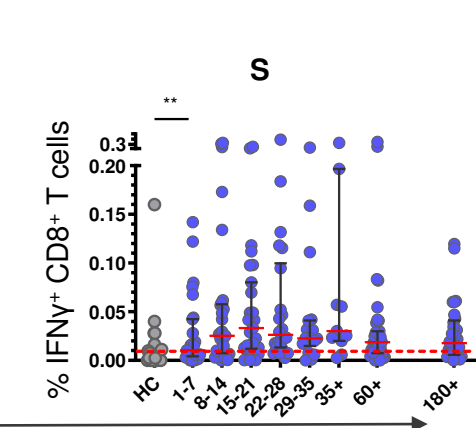
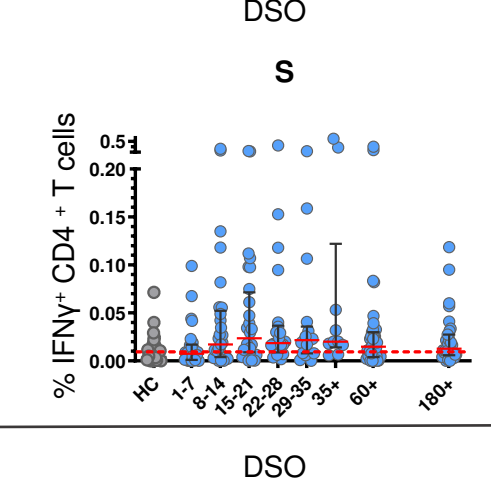
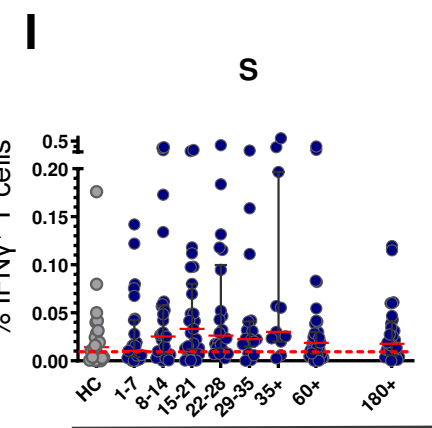
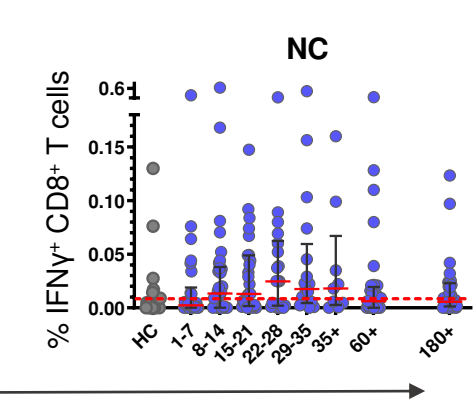
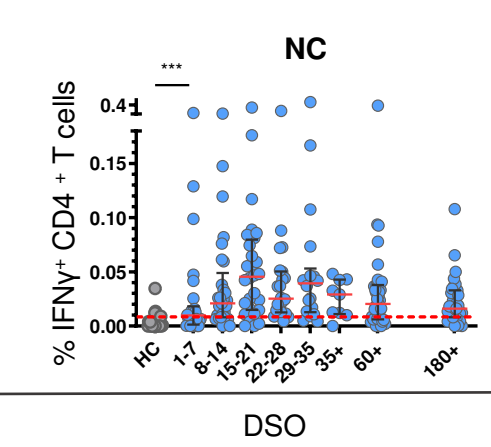
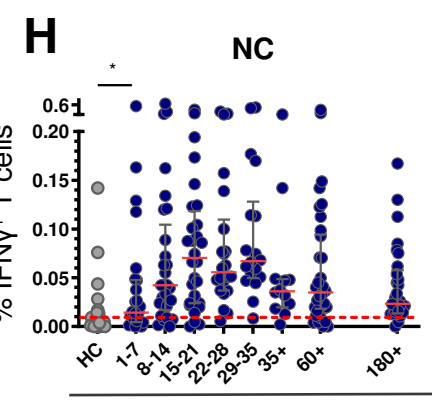
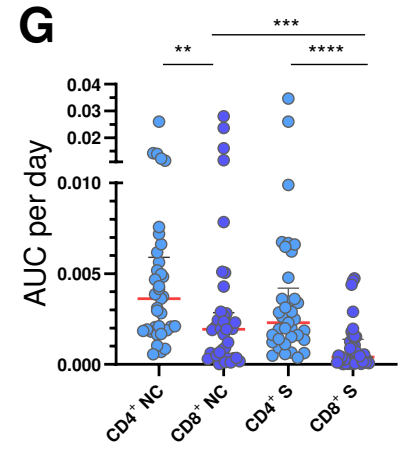
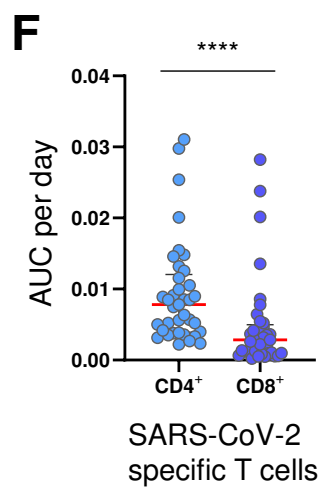
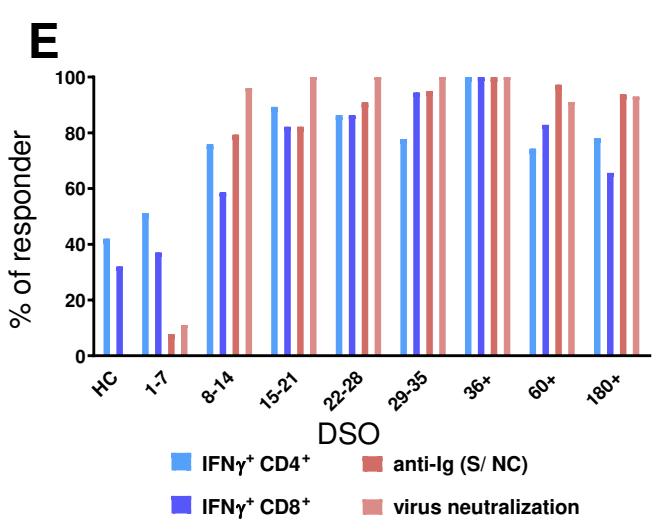
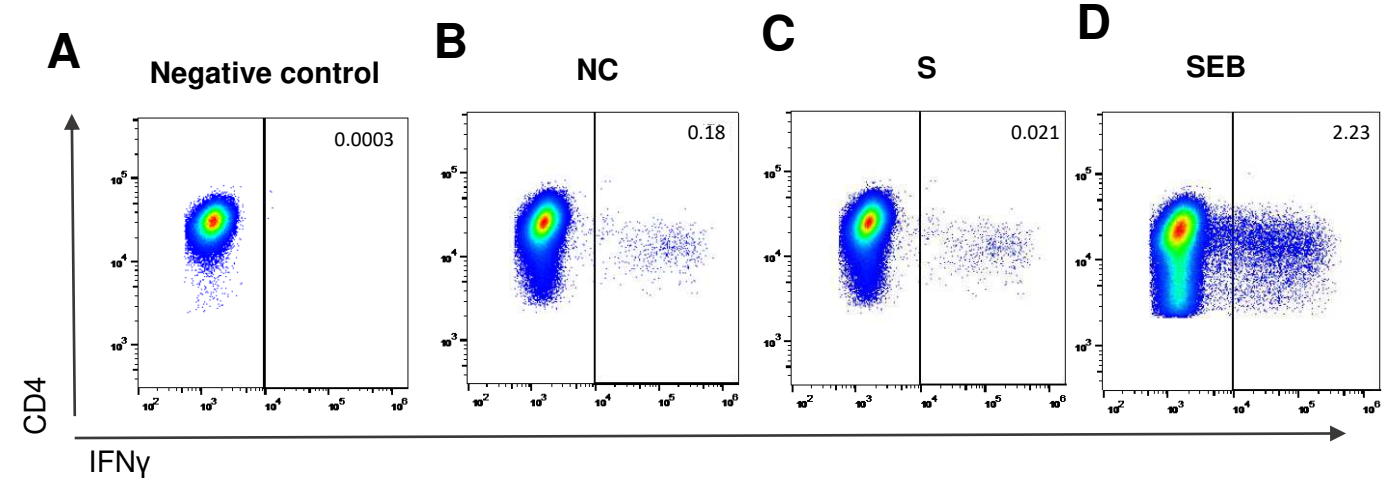


Figure 1 . Study overview, upper airways viral loads, and antibody-mediated neutralization of SARS-CoV-2. (A) Longitudinal quantification of upper airways viral loads (UA-VLs) in patients with mild COVID-19 (n = 25) recruited during the first week of symptom onset. Each line represents one donor. DSO, days since symptom onset. **(B)** Pseudovirus neutralization titers (ID₅₀). Each dot represents one donor. The cutoff is indicated by the dotted red line. Serum samples that did not achieve 50% neutralization (ID₅₀ < 10) were assigned a value halfway below the lower limit of quantification (ID₅₀ = 5). Data are shown as median ± IQR **(B)**.



DSO

Figure 2. T cell responses against the nucleocapsid and spike proteins of SARS-CoV-2. (A–D) Representative flow cytometry plots showing the identification of IFN- γ ⁺ CD4⁺ T cells in the absence of stimulation (A) or in the presence of overlapping nucleocapsid (NC) peptides (B), overlapping spike (S) peptides (C), or staphylococcal enterotoxin B (SEB) as the positive control (D). Plots are gated on CD3. Numbers indicate the percent frequency of CD4⁺ T cells that produced IFN- γ . (E) Responder frequencies for IFN- γ ⁺ CD4⁺ and IFN- γ ⁺ CD8⁺ T cells specific for NC or S, antibody titers against NC or S, and antibody-mediated neutralization of SARS-CoV-2. DSO, days since symptom onset; HC, healthy control. (F, G) Area under the curve (AUC) per day comparisons of the overall magnitude of SARS-CoV-2-specific CD4⁺ versus CD8⁺ T cells (F) and the overall magnitude of SARS-CoV-2-specific CD4⁺ versus CD8⁺ T cells broken down by target protein (NC versus S). Each dot represents one donor. (H) Frequencies of all NC-specific T cells (left), NC-specific CD4⁺ T cells (middle), and NC-specific CD8⁺ T cells (right). Each dot represents one donor. The cutoff is indicated by the dotted red line. (I) Frequencies of all S-specific T cells (left), S-specific CD4⁺ T cells (middle), and S-specific CD8⁺ T cells (right). Each dot represents one donor. The cutoff is indicated by the dotted red line. Data are shown as median \square IQR (F, G, H, and I). * $p < 0.05$, ** $p < 0.01$, *** $p < 0.001$, **** $p < 0.0001$ (Mann-Whitney U test or Wilcoxon signed rank test).

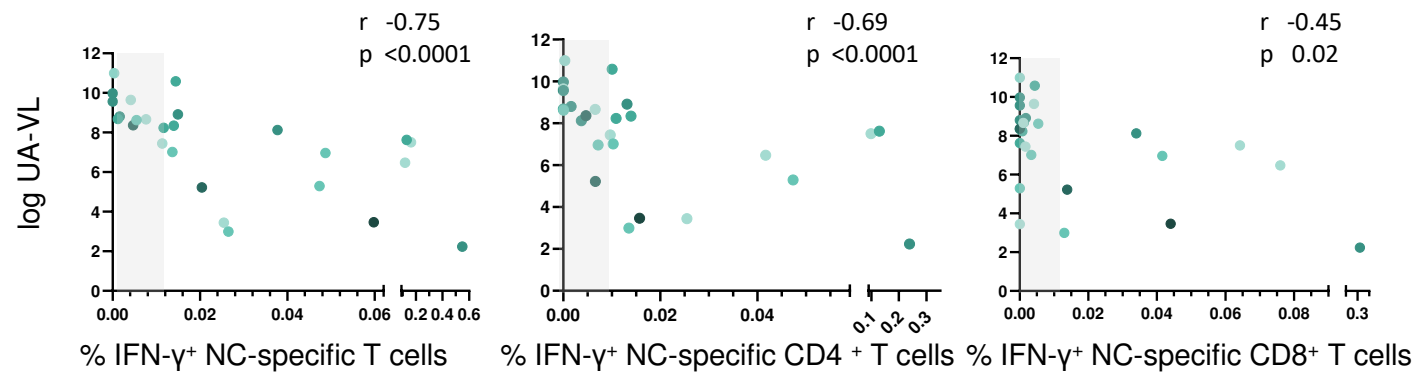
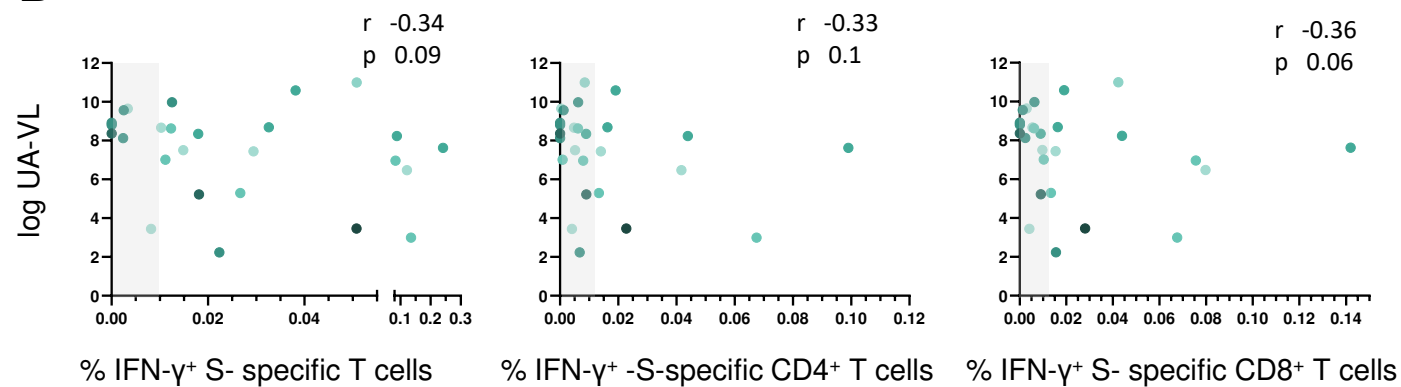
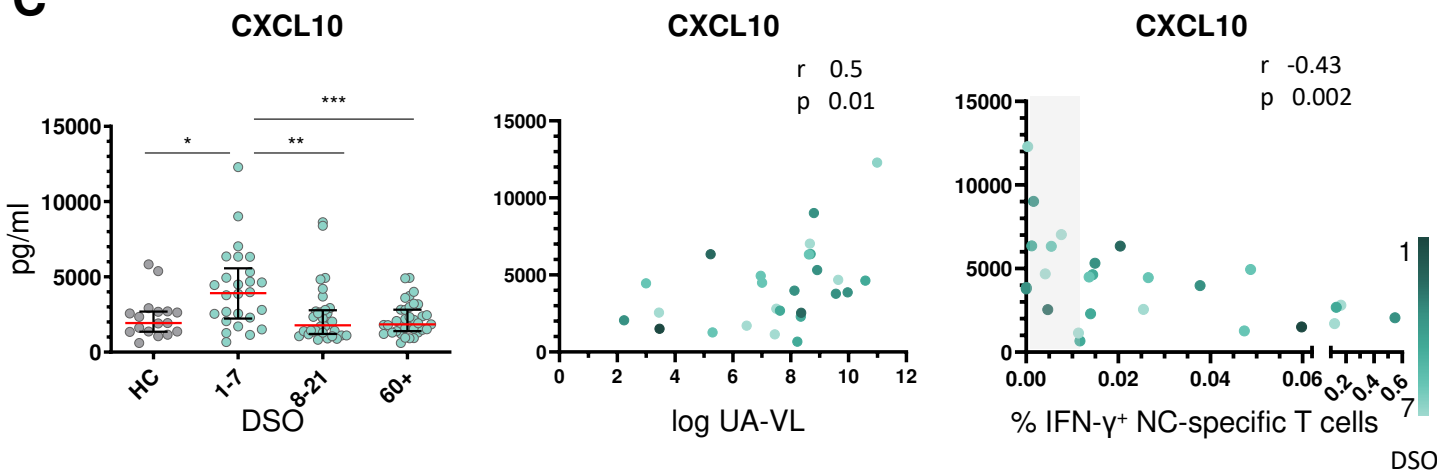
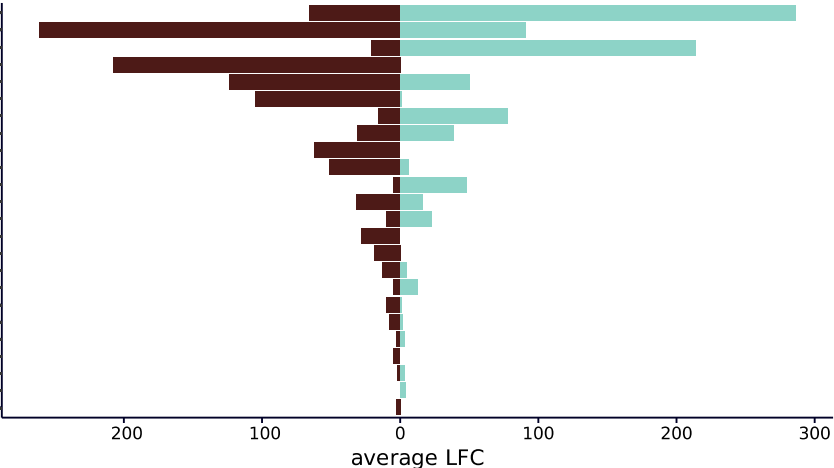
A**B****C**

Figure 3. Nucleocapsid-specific T cell responses correlate inversely with upper airways viral loads and systemic markers of inflammation during acute infection with SARS-CoV-2. (A, B) Spearman rank correlations showing upper airways viral loads (UA-VLs) versus the frequencies of all NC-specific T cells (left), NC-specific CD4 $^+$ T cells (middle), or NC-specific CD8 $^+$ T cells (right) (A) and the frequencies of all S-specific T cells (left), S-specific CD4 $^+$ T cells (middle), or S-specific CD8 $^+$ T cells (right) (B) during the first week after symptom onset. (C) Left: plasma concentrations of CXCL10 are shown for healthy controls (HCs) and longitudinally for patients according to the number of days since symptom onset (DSO). Data are shown as median IQR. Middle and right: Spearman rank correlations showing plasma concentrations of CXCL10 during the first week after symptom onset versus UA-VLs (middle) and the frequencies of all NC-specific T cells (right). The gray bar indicates non-responders (right). * $p < 0.05$, ** $p < 0.01$, *** $p < 0.001$ (Mann-Whitney U test).

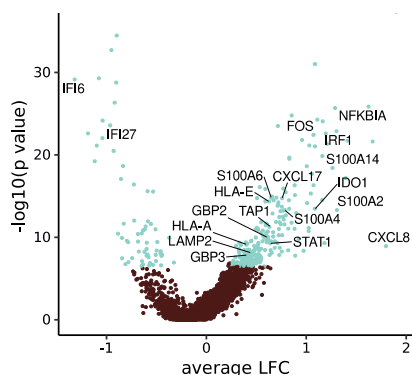
Figure 4. Gene expression profiles in immune cell subsets during acute infection with SARS-CoV-2. RNA sequencing data were obtained from circulating CD4⁺ T cells (light blue), CD8⁺ T cells (dark blue), monocytes (light green), and NK cells (dark green) isolated during the first week after symptom onset (n = 14 patients with mild COVID-19). **(A)** Spearman rank correlations showing mean expression scores for *OAS1* (left), *STAT1* (middle), and *PKR* (right) versus IFN- γ ⁺ CD4⁺ (squares) and IFN- γ ⁺ CD8⁺ T cell frequencies (triangles) and upper airways viral loads (circles, UA-VLs). Whiskers show 95% confidence intervals calculated using bootstrapping with replacement using sample numbers equal to the original data set. **(B–D)** Spearman rank correlations showing mean pathway expression scores for CD4⁺ T cells versus IFN- γ ⁺ CD4⁺ T cell frequencies **(B)**, CD8⁺ T cells versus IFN- γ ⁺ CD8⁺ T cell frequencies **(C)**, and monocytes versus UA-VLs **(D)**. Data are shown as r values with 95% confidence intervals. **(E)** Spearman rank correlations were calculated for all KEGG pathways in the categories *Signal Transduction*, *Signaling Molecules and Interaction*, *Immune System*, and *Cell Growth and Death* (KEGG database). Data are shown as z-normalized mean pathway expression scores restricted to r values above 0.25 or below -0.25. Patients were clustered by expression profile similarity. Pathways are shown for cell subsets with significant gene set enrichment analysis scores (top row, p < 0.05).

A

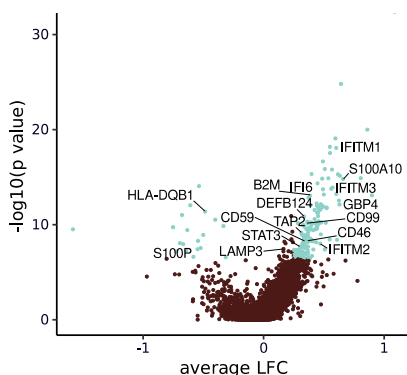
- Developing ciliated cells
- FOXJ1 high ciliated cells
- Interferon responsive ciliated cells
- Early response T cells
- Early response FOXJ1 high ciliated cells
- SCGB1A1 high goblet cells
- AZGP1 high goblet cells
- SPRR2D high squamous cells
- BPIFA1 and chemokine high secretory cells
- Early response secretory cells
- CD8 T cells
- CCL5 high squamous cells
- Interferon responsive secretory cells
- MUC5AC high goblet cells
- Deuterosomal cells
- BEST4 high cilia high ciliated cells
- SERPINB11 high secretory cells
- Basal cells
- BPIFA1 high secretory cells
- Cilia high ciliated cells
- Ionocytes
- KRT24 KRT13 high secretory cells
- VEGFA high squamous cells
- Developing secretory and goblet cells



B Developing ciliated cells



Interferon-responsive ciliated cells



CD8+ T cells

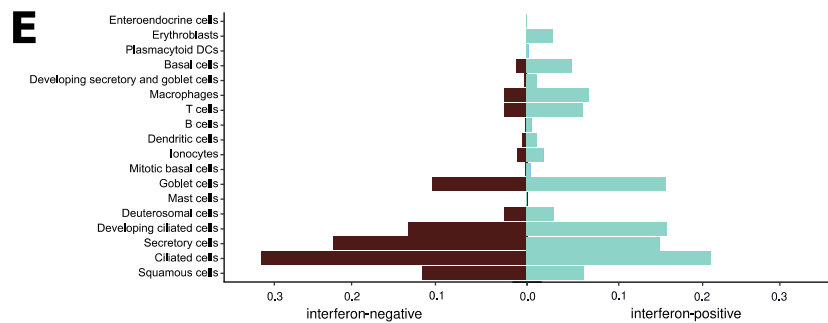
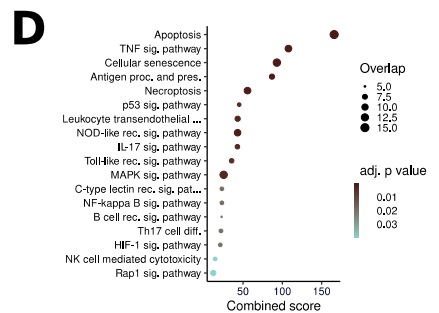
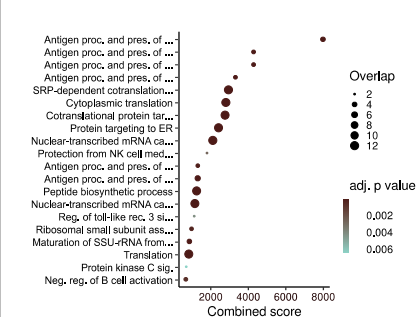
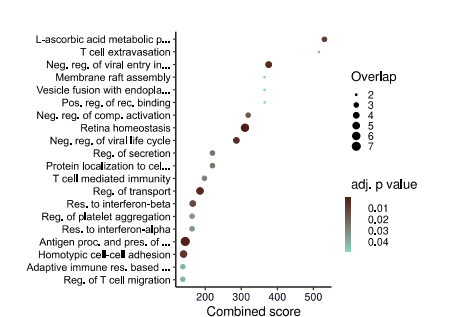
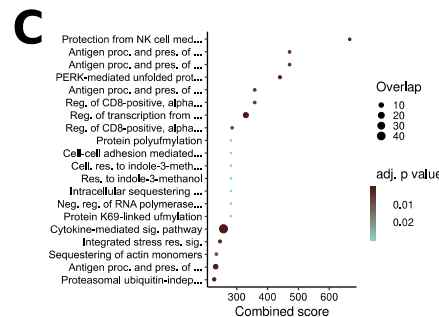
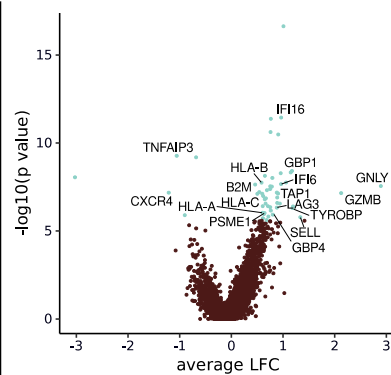
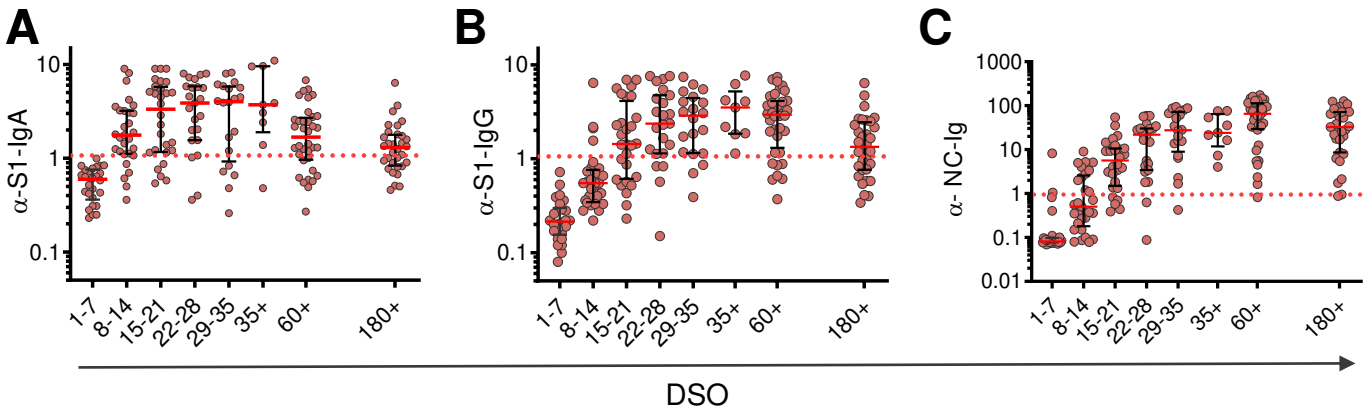
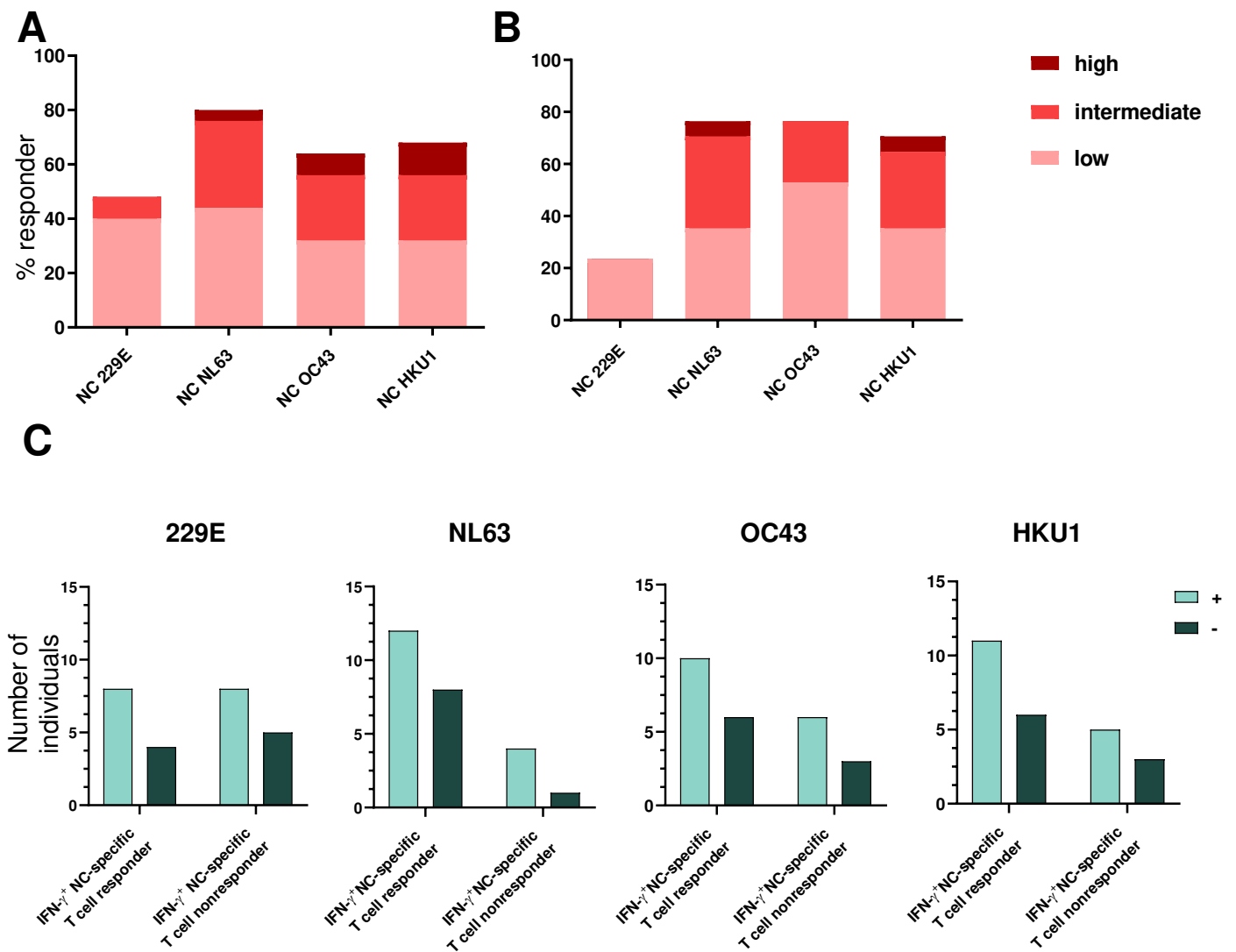


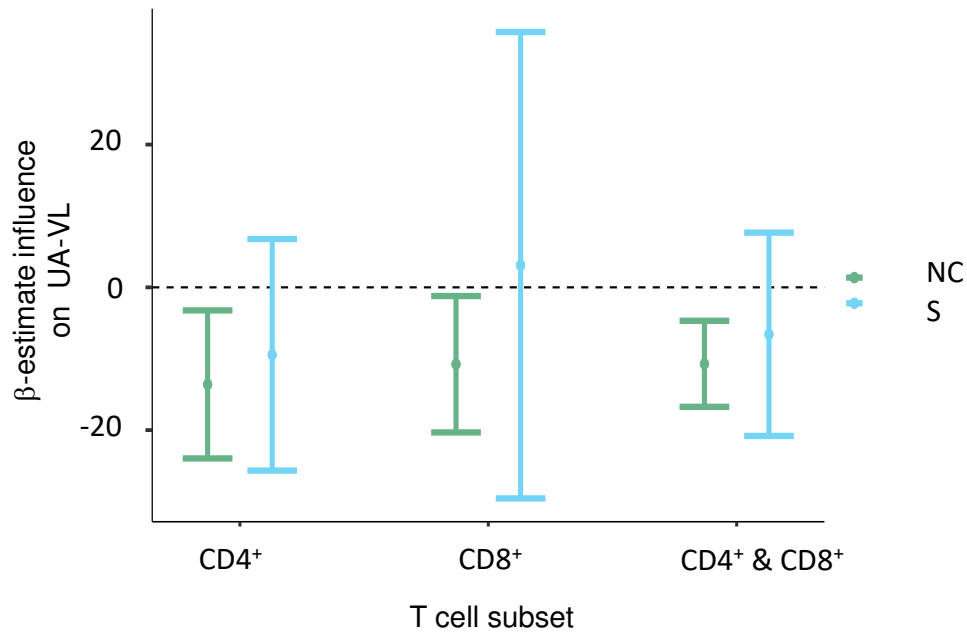
Figure 5. The presence of IFN- γ ⁺ T cells in the upper airways is linked with antigen presentation and viral control during acute infection with SARS-CoV-2. (A) Numbers of differentially expressed genes (DEGs) among cell clusters isolated from the nasopharynx (total n = 16 patients with mild to severe COVID-19). (B) Volcano plots showing DEGs (blue) for the indicated cell types (adjusted p < 0.05). (C) Gene ontology (GO) terms enrichment plots (top 20) for the indicated cell types based on a log-fold change (LFC) of 0.25 in either direction (adjusted p < 0.01). Dot size represents the number of genes per term per cell type, and adjusted p values are colored according to the key. (D) As in (C) for developing ciliated cells based on KEGG pathways instead of GO terms. (E) Changes in cell type frequencies for patients with (n = 7) or without (n = 9) T cell expression of IFN- γ . Expression of IFN- γ was considered in CD4⁺ T cells only for analyses of CD8⁺ T cells. All cell types were defined according to the original annotation, except for CD8⁺ T cells, which were reclassified in house.



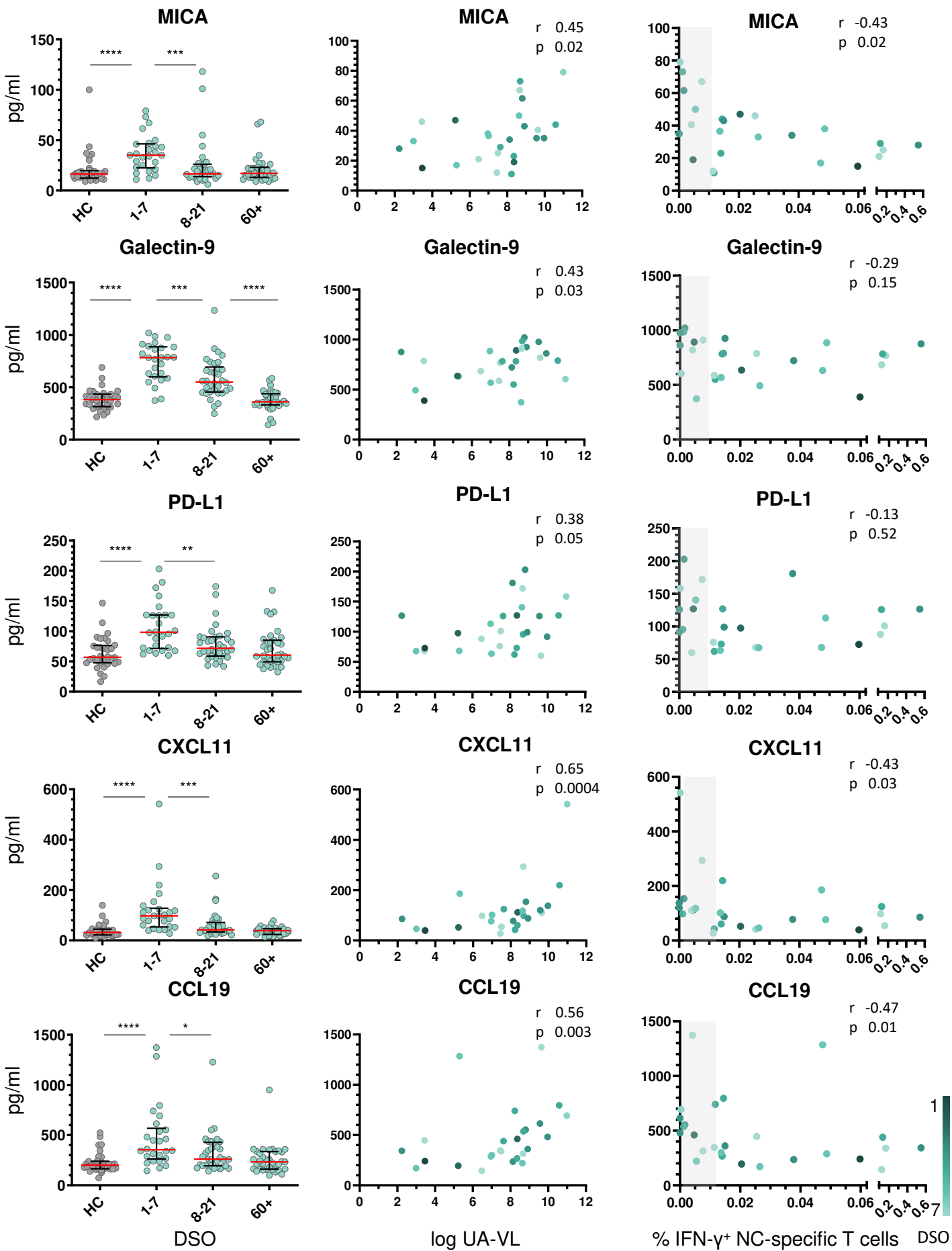
Supp. Figure 1 Supplementary Figure 1. Dynamics of antibody responses against SARS-CoV-2. (A–C) Antibody response dynamics are shown for S-specific IgA (ratio versus internal assay standard) (A), S-specific IgG (ratio versus internal assay standard) (B), and NC-specific total Ig in plasma (arbitrary units) (C). The cutoff for each assay is indicated by the dotted red line. Data are shown as median IQR. DSO, days since symptom onset.



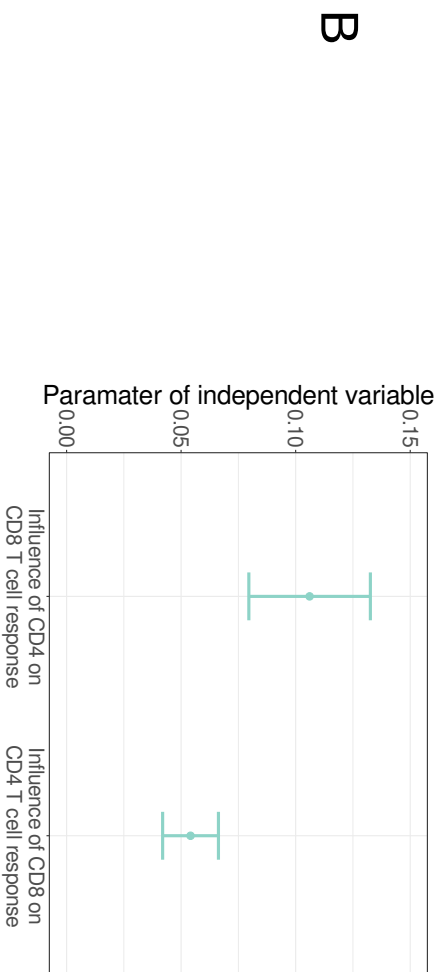
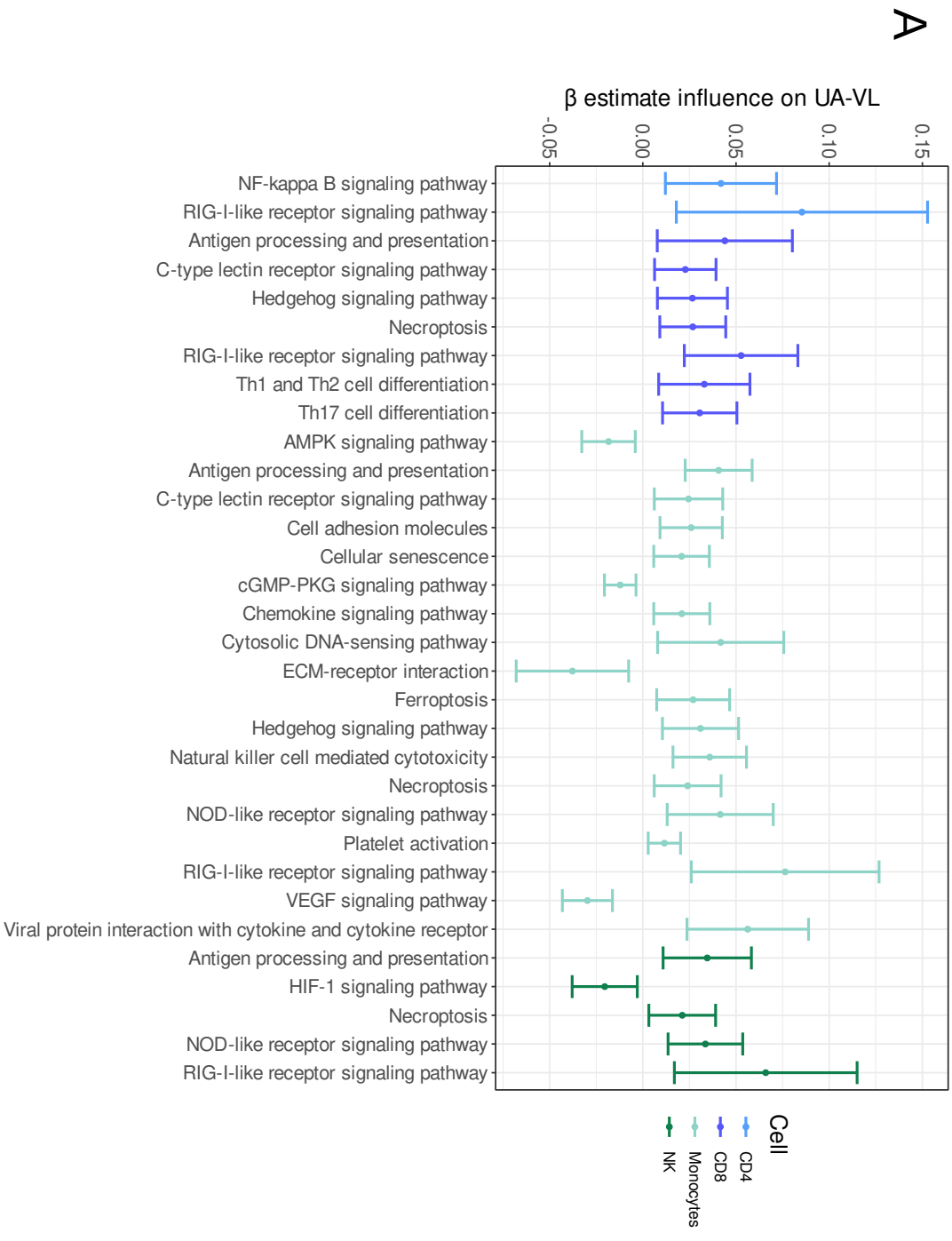
Supp. Figure 2Supplementary Figure 2. Antibody responses against common cold coronaviruses. (A) Percent frequencies of responders ($n = 25$) with high (dark red), intermediate (red), and low NC-specific antibody responses (pink) against each of the four common cold coronaviruses (CCCVs) during the first week after symptom onset. **(B)** Percent frequencies of non-vaccinated healthy controls ($n = 25$) with high (dark red), intermediate (red), and low NC-specific antibody responses (pink) against each of the four CCCVs. **(C)** Numbers of responders and non-responders with (light green) or without CCCV seroreactivity (dark green) during the first week after symptom onset



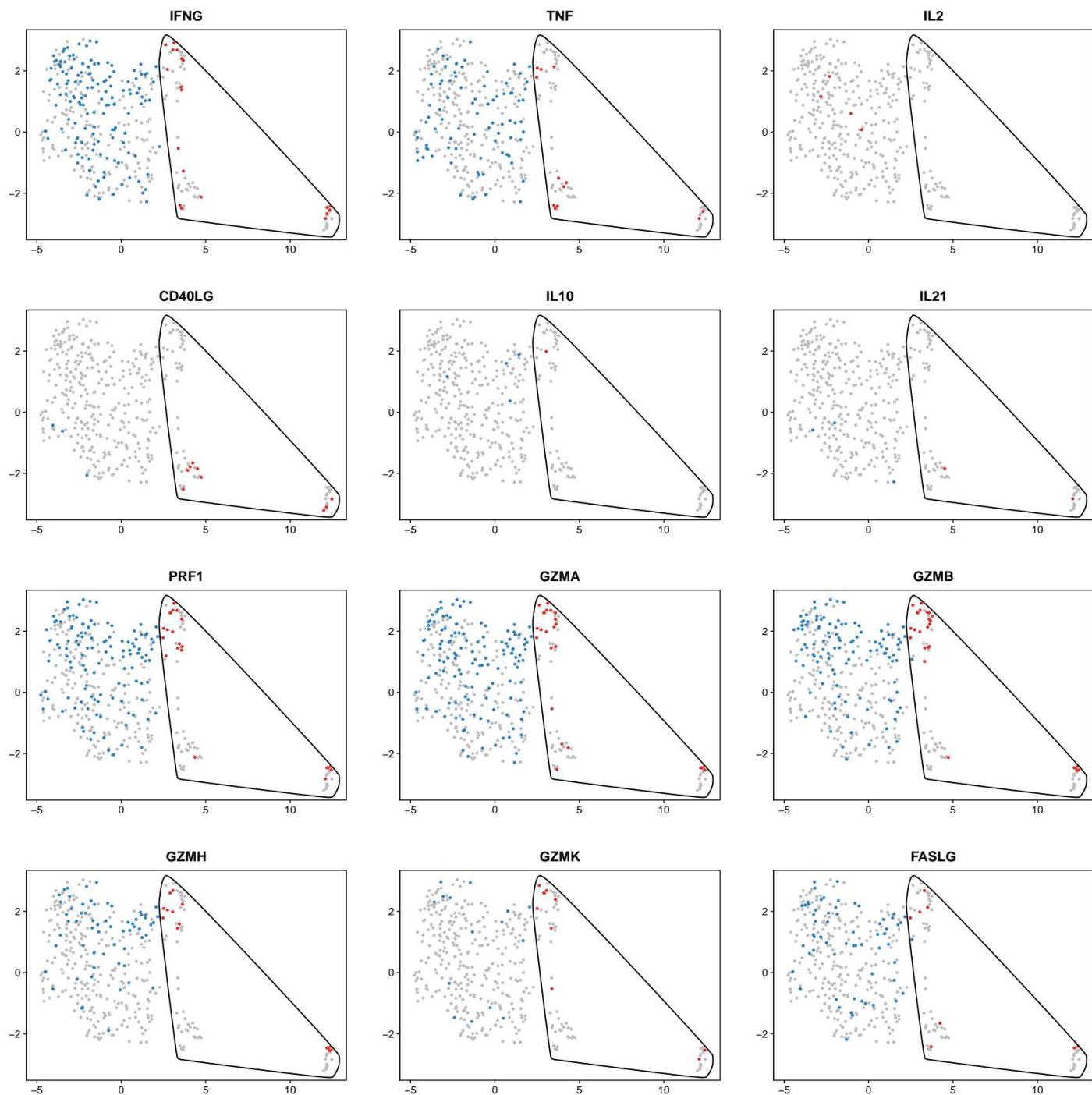
Supp. Figure 3 Supplementary Figure 3. Nucleocapsid-specific CD4⁺ and CD8⁺ T cell responses incrementally reduce the upper airways burden of SARS-CoV-2. Summary of a censored linear mixed effects model showing the possible influence of SARS-CoV-2-specific T cells on upper airways viral loads (UA-VLs). Results are shown as β -estimates with confidence intervals for NC-specific (green) and S-specific T cells (blue).



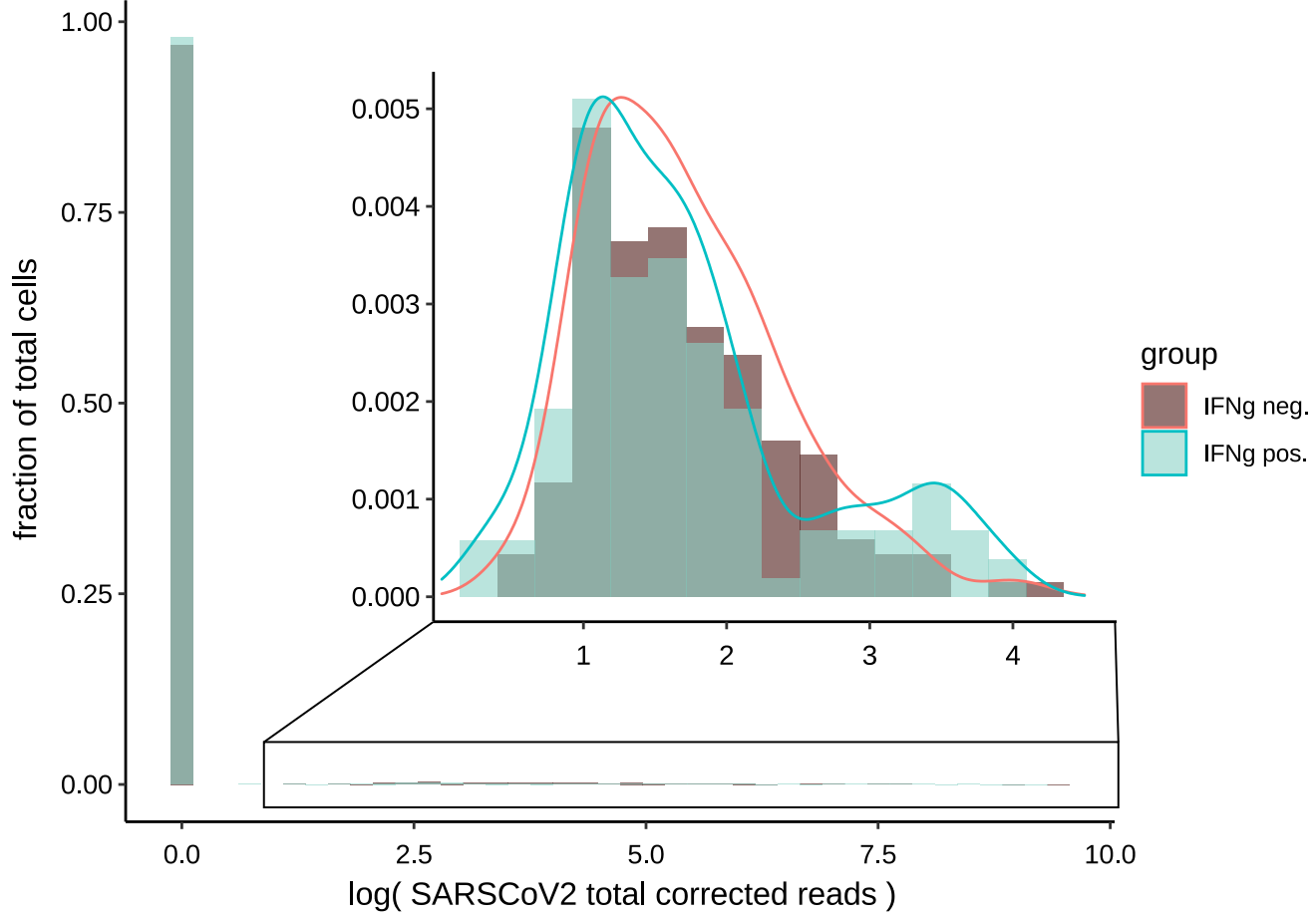
Supplementary Figure 4. Dynamics of plasma soluble factors after infection with SARS-CoV-2. Left: plasma concentrations of MICA, galectin-9, PD-L1, CXCL11, and CCL19 are shown for healthy controls (HC, n = 25) and longitudinally for patients (n = 37) according to the number of days since symptom onset (DSO). Data are shown as median IQR. Middle: Spearman rank correlations showing plasma soluble factors versus upper airways viral loads (UA-VLs) during the first week after symptom onset (key). Right: Spearman rank correlations showing plasma soluble factors versus nucleocapsid (NC)-specific T cell frequencies during the first week after symptom onset (key). *p < 0.05, **p < 0.01, ***p < 0.001, ****p < 0.0001 (Mann-Whitney U test).



Supp. Figure 5. Modeling interactions between upper airways viral loads and activation of immune pathways in circulating immune cell subsets controlled for the influence of NC-specific T cell responses. (A) beta-estimates for the interaction between upper airways viral loads (UA-VLs) and selected immune pathway scores achieving significance ($p < 0.05$). Dots indicate point estimates, and whiskers indicate 95% confidence intervals, computed using normal approximations. Results are clustered according to immune cell subsets (key). (B) Expected influence of NC-specific CD4⁺ T cells on NC-specific CD8⁺ T cell responses (left) and vice versa (right). Estimates were obtained using two separate linear mixed effect



Supp. Figure 6 Supplementary Figure 6. Gene expression of selected cytokines and cytotoxic effector molecules in nasopharyngeal T cells during acute infection with SARS-CoV-2. Expression of the indicated genes is shown for nasopharyngeal CD4⁺ T cells (inside the drawn gate) and nasopharyngeal CD8⁺ T cells (outside the drawn gate). Red dots indicate nasopharyngeal CD4⁺ T cells expressing the indicated gene, and blue dots indicate nasopharyngeal CD8⁺ T cells expressing the indicated gene.



Supp. Figure 7. Influence of IFN- γ on intracellular SARS-CoV-2 RNA. The graph shows the distribution of the logarithm of total corrected read counts of intracellular SARS-CoV-2 RNA in responders (blue) and non-responders (red). Responders were characterized by lower counts and greater numbers of cells without SARS-CoV-2 RNA. The effect was significant ($p = 0.00013$).